Streaming potential dependence on water-content in Fontainebleau sand

Vincent Allègre, Laurence Jouniaux, François Lehmann, Pascal Sailhac

submitted to *Geophys. J. Int.*

Streaming potential dependence on water-content in Fontainebleau sand

V. Allègre[1], L. Jouniaux[1], F. Lehmann[2] and P. Sailhac[1]

[1]*Institut de Physique du Globe de Strasbourg, UdS-CNRS UMR 7516*

Université de Strasbourg, 5 rue rené Descartes, 67084, Strasbourg, FRANCE

[2]*Laboratoire d'Hydrologie et de Géochimie de Strasbourg, UdS-CNRS UMR 7517*

Université de Strasbourg, 1 rue Blessig, 67000, Strasbourg, FRANCE

Key words: electrokinetics, streaming potential, self potential, water saturation, unsaturated flow, water content

SUMMARY

The electrokinetic potential results from the coupling between the water flow and the electrical current because of the presence of ions within water. The electrokinetic coupling is well described in fluid-saturated media, however its behaviour under unsaturated flow conditions is still discussed. We propose here an experimental approach to investigate streaming potential variations in sand at unsaturated conditions. We present for the first time continuous records of the electrokinetic coefficient as a function of water content. Two drainage experiments have been performed within a column filled with a clean sand. Streaming potential measurements are combined with water pressure and water content measurements every 10 centimeters along the column. In order to model hydrodymanics during the experiments, we solve Richards equation coupled with an inverse problem to estimate the hydraulic parameters of the constitutive relations between

hydraulic conductivity, water pressure and water content. The electrokinetic coefficient C shows a more complex behaviour for unsaturated conditions than it was previously reported and cannot be fitted by the existing models. The normalized electrokinetic coefficient increases first when water saturation decreases from 100% to about 65% - 80%, and then decreases as the water saturation decreases, whereas all previous works described a monotone decrease of the normalized electrokinetic coupling as water saturation decreases. We delimited two water saturation domains, and deduced two different empirical laws describing the evolution of the electrokinetic coupling for unsaturated conditions. Moreover we introduce the concept of the electrokinetic residual saturation $S_w^{r,ek}$, which allows us to propose a new model derived from the approach of the relative permeability used in hydrodynamics.

1 INTRODUCTION

The Self-Potential (SP) method is a passive geophysical method based on the natural occurrence of electric fields on the earth's surface. The SP anomalies are usually explained by the electrokinetic, electrochemical, and thermoelectric effects (Marshall & Madden 1959). Therefore the SP method has been used for a variety of geophysical applications. The SP method has been used to image contaminant plumes (Naudet et al. 2003), and to detect salt concentration fronts (Maineult et al. 2004, 2005). Numerous SP observations are interpreted through the electrokinetic coupling, for instance to characterize geothermal and volcanic areas (Finizola et al. 2002, 2004). However the electrokinetic origin involved to explain the positive SP anomalies observed on active volcanoes is still under debate (Ishido 2004; Onizawa et al. 2009).

Recent models on electrokinetics have been proposed for reservoir geophysics and petroleum investigations (Saunders et al. 2008; Jackson 2008), and self-potentials have been monitored

during hydraulic tests in boreholes (Marquis et al. 2002; Darnet et al. 2006; Maineult et al. 2008). Moreover recent developments allow us to use SP measurements in boreholes as an electrical flowmeter (Pezard et al. 2009). The electrokinetic coupling is also directly involved in seismo-electromagnetic effects (Pride 1994; Garambois & Dietrich 2001, 2002; Bordes et al. 2006; Strahser et al. 2007; Bordes et al. 2008).

For hydrological applications, Bogolovsky & Ogilvy (1970) described a method to infer water table variations from self-potential measurements. Moreover, the inversion of SP observations can yield an estimate of the vadose zone hydraulic properties (Sailhac & Marquis 2001; Gibert & Pessel 2001; Darnet et al. 2003; Sailhac et al. 2004; Titov et al. 2005). However inferring a firm link between SP intensity and water flux (Jouniaux et al. 1999; Doussan et al. 2002; Darnet & Marquis 2004) or deformation (Henry et al. 2003; Jouniaux et al. 1994) is difficult, although it has been proposed to predict permeability using electrokinetic theory (Glover et al. 2006; Glover & Walker 2009).

Electrokinetic contribution to self-potentials takes its origin in the electrical double-layer (EDL), or electrical triple-layer (Davis et al. 1978), which is located at the electrolyte/grain interface of a saturated porous media. This concept has been first introduced by Stern (1924), and then modeled and improved by electrochemists (Overbeek 1952; Dukhin & Derjaguin 1974). The electrokinetic coefficient is defined as the ratio between the macroscopic induced electrical potential and the driving pore pressure. Indeed the water flow carries the ions present in the water and can induce an electrical current. The electrokinetic coefficient depends on some fluid parameters, as electrical conductivity and dynamic viscosity, and on the so-called zeta potential (ζ) (Smoluchowski 1905), which is the the electrical potential at the shear plane of the EDL. Its understanding is crucial for electrokinetics. The ζ potentials inferred from streaming potential measurements on crushed samples have been reported as a function of pH (Ishido & Mizutani 1981; Hase et al. 2003), temperature (Ishido & Mizu-

tani 1981; Tosha et al. 2003), and mineral composition (Massenet & Pham 1985; Morgan et al. 1989; Pozzi & Jouniaux 1994; Guichet et al. 2006). The influence of the fluid electrical conductivity has also been investigated (Pride & Morgan 1991; Lorne et al. 1999a; Jouniaux et al. 2000). It is usually reported that variations of electrical conductivity from 0.001 $S.m^{-1}$ to 1 $S.m^{-1}$ induces a three orders of magnitude change of the electrokinetic coefficient.

However, the variation of the electrokinetic coefficient with saturation is still discussed and not yet understood. The interpretation of SP observations applied to reservoir geophysics requires a good estimation of the electrokinetic coefficient in unsaturated conditions (Jackson 2008; Maineult et al. 2008). Moreover the influence of water content on seismoelectromagnetics is still not known. Experimental measurements on streaming potentials as a function of water content within sand showed that the electrokinetic coefficient decreases when water saturation decreases (Guichet et al. 2003) and showed that this coefficient is roughly linearly dependent on the effective water saturation. Perrier & Morat (2000) suggested a model in which the electrokinetic coefficient is dependent on a relative permeability model. Linde et al. (2007) and Revil et al. (2007) proposed a theroretical model describing the electrokinetic coefficient, based on a relative permeability model too. These two models suggest that the electrokinetic coefficient decreases with decreasing water saturation, however its dependence on water saturation was not found to be linear. Recently Jackson (2008) suggested that the electrokinetic coefficient depends on water saturation as a power law. Few experimental studies have been published on this subject. Since continuous records of the electrokinetic coefficient as a function of water saturation have not been published, to our knowledge, we developed an experimental setup which allows to acquire several independently continuous records of the streaming potential as a function of water saturation. We discuss our results in light of the previous available models and experimental data.

Unsaturated flow occuring in the vadose zone are relatively complex and depends on param-

eters such as water pressure, water content and hydraulic conductivity. Moreover, both the retention relation, which links water pressure to water content (Brooks & Corey 1964), and the relation between hydraulic conductivity and water content (Mualem 1976a) are strongly non linear. The equation describing variations of these hydraulic parameters and water flow in unsaturated conditions was proposed by Richards (1931). The understanding of the hydrodynamics is essential before undertaking the study of the electrokinetic coefficient in unsaturated conditions.

In this work, several drainage experiments were performed, monitoring streaming potentials, water pressure, water content, and cumulative outflow in sand. Using the water pressure and the water-content measurements, we deduced the hydrodynamic parameters of the retention model and hydraulic conductivity model by inversion. Then the water pressure was calculated with a better signal to noise ratio than the measured one. The electrokinetic coefficient was deduced from the streaming potential measurements and from the computed total water pressures as a function of the measured water-content.

2 THEORETICAL BACKGROUND

2.1 Electrokinetic phenomena

Using near-equilibrium thermodynamics (Onsager 1931), and neglecting temperature and concentration gradients, one can write coupling relations which link both the macroscopic electrical ($\mathbf{J}$) and hydrological ($\mathbf{q}$) fluxes to their driving forces; the macroscopic electrical potential gradient, ∇V [V.m^{-1}] and the macroscopic total water pressure gradient ∇P [Pa.m^{-1}],

$$\begin{bmatrix} \mathbf{J} \\ \mathbf{q} \end{bmatrix} = \begin{bmatrix} L_{11} & L_{12} \\ L_{21} & L_{22} \end{bmatrix} \cdot \begin{bmatrix} \boldsymbol{\nabla} V \\ \boldsymbol{\nabla} P \end{bmatrix} \tag{1}$$

Analysing equation 1, the Ohm's law implies $L_{11} = \sigma_r$, with σ_r the bulk electrical conductivity [S.m^{-1}]. Moreover, Darcy's law implies $L_{22} = k/\eta_w$, where k [m^2] is the permeability of the medium and η_w [Pa.s] the dynamic viscosity of the fluid. The streaming current associated with the driving pressure through the electrokinetic coupling, is induced by an excess of charges in the diffuse part of the EDL. The electrokinetic coupling L_{12} is related to the electrokinetic coefficient C [V.Pa^{-1}] as $L_{12} = -C\sigma_r$ [A.Pa^{-1}.m^{-1}]. If the porous medium is water saturated, C will be written as C_{sat}. Consequently, the coupled equation for the electrical current density can be written

$$\mathbf{J} = -\sigma_r \boldsymbol{\nabla} V + C_{sat}\sigma_r \boldsymbol{\nabla} P \tag{2}$$

One can write the conservation of the electrical current density,

$$\boldsymbol{\nabla}.\ \mathbf{J} = -\frac{\partial \rho}{\partial t} \tag{3}$$

with ρ the surface charge density [C.m^{-2}]. For geological materials, one classically assume steady-state with $\partial\rho/\partial t = 0$, thus there remains only the left-hand term of equation 2, with divergence operator $\boldsymbol{\nabla}.\ \mathbf{J} = 0$. Therefore, using equation 2 and integrating equation 3 in the case of a unidirectional flow through a cylindrical saturated porous capillary, one can derive the well known Helmholtz-Smoluchowski (Smoluchowski 1905) relation of the saturated electrokinetic coefficient:

$$C_{sat} = \frac{\Delta V}{\Delta P} = \frac{\epsilon_0 \epsilon_r \zeta}{\eta_w \sigma_w} \tag{4}$$

with the fluid electrical permittivity $\epsilon_0\epsilon_r$ [F.m^{-1}], the fluid dynamic viscosity η_w [Pa.s], the fluid electrical conductivity [S.m^{-1}] and ζ [V], the zeta potential described as the electrical potential inside the EDL at the shear plane. The electrokinetic coefficient can be deduced by applying a driving pressure and by measuring the induced electrical potential. The total water pressure P [Pa] must be considered as the combination of capillary and gravity effects:

$P = \rho_w g(h - z)$ where ρ_w is the density of the fluid [kg.m^{-3}], g is gravity [m.s^{-2}], h is the pressure head [m] and z is the elevation [m].

2.2 Unsaturated flow equations

Considering the mass conservation equation and general form of Darcy's law in 1D leads to the mixed form of Richards equation (Richards 1931), which describes unsaturated water flow in a porous medium,

$$\frac{\partial \theta(h)}{\partial t} - \frac{\partial}{\partial z}\left[K(h)\frac{\partial h}{\partial z} - K(h)\right] = 0 \tag{5}$$

where h is the pressure head [m], K is the hydraulic conductivity [m.s^{-1}] as a funtion of θ or h, t is time [s], and z the distance from the reference altitude [m]. The vertical coordinate z is defined to be positive downward, and the reference elevation is set so that $z = 0$ corresponds to the top of the column. The symbol θ represents the volumetric water content (or moisture content) [m^3.m^{-3}].

Hydraulic conductivity and pressure head depend non-linearly on water content. The $\theta(h)$ and $K(\theta)$ relations are assumed respectively using the Brooks & Corey (1964) model,

$$Se = \frac{\theta - \theta_r}{\theta_s - \theta_r}\begin{cases} \left(\dfrac{h_a}{|h|}\right)^{\lambda} & ,\text{if } \dfrac{h_a}{|h|} < 1 \\ 1 & ,\text{if } \dfrac{h_a}{|h|} > 1 \end{cases} \tag{6}$$

and the Mualem (1976a) model,

$$K(S_e) = K_s.{S_e}^{L+2+\frac{2}{\lambda}} \tag{7}$$

with S_e the effective water saturation defined by,

$$S_e = \frac{\theta - \theta_r}{\theta_s - \theta_r} \tag{8}$$

or by,

$$S_e = \frac{S_w - {S_w}^r}{1 - {S_w}^r} \tag{9}$$

In equation 6, $\theta_s = \phi$ is the water content in saturated conditions with ϕ the porosity, and θ_r is the residual water content which represents the water fraction adsorbed to the matrix grains when the medium becomes highly unsaturated. The parameter K_s is the hydraulic conductivity at saturation [m.s^{-1}], S_w is the water saturation, and is linked to the water content by : $S_w = \theta/\phi$. Thus the residual adsorbed water saturation is defined as ${S_w}^r = \theta_r/\phi$. The air entry pressure is h_a [m], which characterize the threshold pressure for water content to begin to decrease during a drainage. The parameter λ is an hydrodynamic parameter depending on the pore size distribution, which classically varies from 0.9 to 3.2 for sands (Haverkamp et al. 1998, 2005; Leij et al. 2005). The parameter L of the equation 7 takes into account the correlation between the pore size and flow tortuosity, it is chosen at $L = 0.5$ which is a classical value in the literature (Mualem 1976a).

Boundary conditions must be applied to Richards equation at the top and the bottom of the system. For the high and low extremity of the profile, which is a vertical 1D cylindrical column of sand, the following boundary conditions on pressure head (Dirichlet) and flux (Neumann) can be assumed,

$$h(z,t) = h_D(t) \quad \text{or} \quad \left(-K(h)\frac{\partial h}{\partial z} + K\right)_{z=0,l} = q_N(t) \tag{10}$$

with z equal to zero or l (the length of the profile). The variables $h_D(t)$ and $q_N(t)$ are respectively the imposed pressure head and net flux. A zero flux (at the top) and an imposed pressure head (at the bottom) are used as boundary conditions in the inversion process for both experiments presented in this paper.

The mixed form of the Richards equation is solved by the standard Galerkin finite element method (Pinder & Gray 1977) with a fully implicit scheme in time. The system of equations obtained is highly non linear. To linearize the equations, the Newton method described in Lehmann & Ackerer (1998) is used.

The inverse problem is solved following a non-linear optimization process. The objective function to be minimized is defined in equation 11. This function is the difference between measured and computed pressure head at each iteration, respectively h_i^{n+1} and $\hat{h}_i^{n+1}$, and/or water content θ_i^{n+1} and $\hat{\theta}_i^{n+1}$.

$$\mathcal{O}(\mathbf{p}) = \sum_{n=0}^{N-1}\sum_{i=1}^{N_m} w_{ih}^{n+1}(h_i^{n+1} - \hat{h}_i^{n+1}(\mathbf{p}))^2 + \sum_{n=0}^{N-1}\sum_{i=1}^{N_m} w_{i\theta}^{n+1}(\theta_i^{n+1} - \hat{\theta}_i^{\,n+1}(\mathbf{p}))^2 \quad (11)$$

The vector $\mathbf{p}$ represents adjusted parameters of the model, h_i^{n+1} and θ_i^{n+1} are the measured pressure head and water content at location i and time $n+1$ respectively. The pressure head and water content $\hat{h}_i^{n+1}$ and $\hat{\theta}_i^{\,n+1}$ are the computed model at iteration i and time $n+1$. Differences between measurements and models are computed in a least-square sense, and weight functions w_{ih} and/or $w_{i\theta}$ are also added. For more details on both forward and inverse problem process mentioned here, see Lehmann & Ackerer (1998) and Hayek et al. (2007). We used this approach to inverse the water pressure and the water-content measurements in order to deduce the unknown hydraulic parameters introduced by equations 6 and 7. Hopmans et al. (2002) explained that pressure measurements during a drainage experiment allow a good estimation of these hydraulic parameters in the inverse approach, without knowing K_s or θ_s. In contrast, they added that these two parameters should be measured and known in the case of measuring only the cumulative water outflow without any pressure measurements. The total water pressures, ΔP are obtained from differences of water pressures, h. The uncertainty on water pressure measurements is almost 1 cm (in terms of water height) or 100 Pa. This uncertainty is too large to infer total water pressure differences (which are only 600 Pa of maximum amplitude in our case) with a good signal to noise ratio. Thus, the computed water pressures, which show a better signal to noise ratio, were used to calculate the total water pressure P. Hence, the electrokinetic coefficients were

deduced from the streaming potential measurements and from computed total water pressure in Section 4.2.

2.3 Electrokinetic coefficient in unsaturated conditions

Since the electrokinetic equations were developed in saturated conditions, the effect of water content on the electrokinetic coupling is still in debate. Sprunt et al. (1994) showed that the streaming potential could be enhanced when bubbles are flowing within the water. It was first proposed that the electrokinetic coefficient was inversely proportional to the effective saturation with a power n, meaning that the electrokinetic coefficient decreases with increasing water saturation (Revil et al. 1999a; Darnet & Marquis 2004; Sailhac et al. 2004). Then the first experimental study on the electrokinetic coefficient behaviour in unsaturated conditions was reported by Guichet et al. (2003). In their work, several drainage experiments were carried out by injecting inert gas into a 1 meter long column filled with water saturated Fontainebleau sand, and streaming potentials and water content were monitored. Their study showed, contrary to predictions, that the electrokinetic coefficient linearly increases with the effective water saturation S_e,

$$C(S_w) = C_{sat} S_e \tag{12}$$

with C_{sat}, the saturated electrokinetic coefficient.

Then Perrier & Morat (2000) suggested that the electrokinetic coefficient depends on a relative permeability model k_r,

$$C(S_w) = C_{sat} \frac{k_r}{{S_w}^n} \tag{13}$$

with k_r a relative permeability model defined as : $k_r = \left((S_w - 0.1)/0.9\right)^2$ (Adler et al. 1997), and assuming that the relative electrical conductivity is equal to S_w^n. The parameter n is the Archie saturation exponent (Archie 1942), and is assumed to be 2 by Perrier & Morat

(2000). This exponent has been observed to be about 2 for consolidated rocks and in the range $1.3 < n < 2$ for coarse-texture sand (Schön 1996; Guichet et al. 2003; Lesmes & Friedman 2006). Note that the use of Archie's law is valid in the absence of surface electrical conductivity.

Recently a new formulation including another relative permeability model was proposed by (Revil et al. 2007),

$$C(S_w) = C_{sat} \cdot \frac{k_r}{{S_w}^{n+1}} \tag{14}$$

assuming that the charge density of the pore space is inversely proportional to the water saturation S_w, and considering the similar behaviour of hydraulic and electrical conductivity for unsaturated conditions. The Mualem relative permeability k_r (Mualem 1976a), introduced by equation 7, is chosen with $L = 1$ instead of $L = 0.5$.

Recently (Saunders et al. 2008) proposed a power law to describe the behaviour of the unsaturated relative electrokinetic coefficient during imbibition,

$$C_r(S_w) = {S_{wn}}^{n_s} \tag{15}$$

This relation, where n_s is a positive exponent between 0.01 and 1, was used in a numerical calculation to compute downhole SP monitoring during the injection of water in oil reservoirs. This expression depends on a particular normalized water saturation given by,

$$S_{wn} = \frac{S_w - S_{wc}}{1 - S_{wc} - S_{ro}} \tag{16}$$

with S_{wc} and S_{ro}, the connate water saturation and oil saturation respectively. Equations 15 and 16 imply the maximum of the relative electrokinetic coefficient to be around $S_w = 80\%$ which had never been reported by experimental studies or theoretical developments up to now. In the present work, only two different phases (water and air) are considered, so that the equation 16 would be strictly equivalent to effective water saturation, $S_{wn} = S_e$.

3 EXPERIMENTAL SETUP

Several drainage experiments in sand were performed using the experimental apparatus depicted in Figure 1. During water flow, streaming potentials are monitored, as well as water pressure, water content, temperature and cumulative outflow. Streaming potentials are measured using 10 non-polarizable silver-silver chloride electrodes placed every 10 cm along the column. Each electrode rod is put into a porous ceramic cup (of 6 mm diameter and 28 mm length), filled with deionized water, which is in contact with the porous medium. These cups remain saturated until a pressure less than 0.1 MPa (or 1 atm) is applied, so that the cups remain electrically conducting. Therefore streaming potential measurements are still possible when the sand is unsaturated. The experimental setup consists of a 1.3 m long and 10 cm diameter plexiglass column. Each SP difference is measured between one electrode and the reference one, located at the bottom of the column. A pressure transmitter is located in the centre of each of the 9 dipoles formed by each pair of consecutive electrodes. These sensors (33 & 35xx, Keller Inc.) are floating piezoresistive transducers, and measure water pressure from -0.07 to 0.07 MPa with almost 100 Pa accuracy. Moreover, water content measurements are combined to water pressure, at the same locations along the column, in order to monitor the dynamic of the water flow. Water content is measured using Theta probes ML2x (Δ-T Devices Ltd.) which are based on medium impedance measurements (Gaskin & Miller 1996). All Theta probes were calibrated using a scale-down of the column, with exactly the same geometry, using nine sand/water mixtures prepared in the whole range of water content (from 0 to θ_s with step of 0.05). Then a calibration model linking the weighted water content to the measured voltage output of the nine probes was deduced. We had also planned to measure the electrical resistivity each 10 cm along the column. Unfortunately all tests performed up to now could not allow us to deduce a correct relation

which links the measured electrical resistance and the true resistivity of the medium. We measured the electrical resistivity as a function of water content by a weighting method to deduce the Archie saturation exponent n, as explained in Appendix B.

We adopt the following protocol for each drainage experiment :

(i) The column was first filled with Fontainebleau sand (Sifraco NE34) saturated with deionized water. As deionized water has a low conductivity, its conductivity increases when it is in contact with the sand. Therefore, the water was forced to circulate through the sand until its conductivity reached a constant value (reported in Table 3), so that the mixture water/sand could be considered in chemical equilibrium.

(ii) Before the drainage begins, a reservoir connected to the bottom of the column (see R1 in Figure 1) was placed at the top level of the column. Thereby, both the sand surface and the surface of water in the reservoir represent of a free pressure surface, so that the medium is in hydrostatic state.

(iii) To start the drainage, the reservoir was moved downwards at the bottom of the column. Thus a hydraulic head difference was applied to the medium at around 1 m of water height which induces the fluid flow. After each experiment, a sample of water was collected to measure its pH and electrical conductivity.

The sand was packed as uniformly as possible, and the most heavily possible in laboratory (see Appendix A). Moreover several drainages are performed before any measurements. Unfortunately no method exists to reproduce the structure of an undisturbed soil. Packing of the column depends on the method used, on the operator and on the scale of the column (Corey 2002). During the whole experiment, until water outflow stopped, streaming potentials, water pressure and water content were recorded every 80 seconds using a HP34970A switch unit (Agilent Technologies) coupled with a HP34901a multiplexer module, remotly

controlled by a computer. This unit provides a internal impedance greater than 10 GΩ. Electrical potential differences were also integrated on 100 periods of the 50 Hz signal, so that each measurement was performed over 2 seconds. This averaging allows the automatic rejection of the 50 Hz anthropogenic electrical noise. We detailed in Appendix A the tests that we performed to ensure that we have measured correctly the streaming potentials. In the next part we will present all the signals measured as a function of time. In addition, petrophysical characteristics of the sand are reported in Table 1. We discuss in this paper two experiments: the first one lasted about two hundred hours, and the second one three hundred hours. These experiments allowed us to obtain independently seven continuous records for the behaviour of the electrokinetic coefficient versus water saturation.

4 EXPERIMENTAL RESULTS

4.1 Hydrodynamic measurements

Water pressures and water-content measurements were used to estimate the hydraulic parameters of the sand K_s, h_a, λ, θ_s and θ_r using the numerical scheme described in Section 2 (equations 6 and 7). Before drainage starts (t $\simeq$ 20h), when the medium is still in hydrostatic equilibrium, a 10 cm pressure head shift between each sensor is observed (see Figure 2a). The dashed and solid lines are the results of the inversion process and fit the measured water pressure head quite well. Measured water saturations begin to decrease one after the other during the drainage, as time progresses (see Figure 2b). This time shift is related to the air entry pressure, defined as h_a, so that a pressure head around -40 cm is required before the water content begins to decrease. The time axis should be interpreted as representing the direction of decreasing water saturation. Thus, curves in Figure 2b characterize the water front propagation within the column, and consequently informs us about the flow dynamics

of the experiment. Estimated values for K_s, h_a, λ, θ_s and θ_r are reported in Table 2. Measured value of K_s is also reported in Table 2. It is slightly greater than the computed K_s considering that the permeability range is over twenty-two orders of magnitude, and still in the classical range for sandy texture soils (Carsel & Parrish 1988). Using measured value or inverted value of K_s lead to the same results for the calculated pressures during the drainage experiments, and fit the measured pressures. The results are in good agreement with classical values in the literature for this kind of medium (Rawls et al. 1982). Figures 2c and 2d show the results for the second experiment. The similarity of the estimated values of K_s, h_a and λ let us conclude that the two experiments are very similar in terms of hydrodynamics. The estimated values of λ are significantly higher than values introduced in Section 2.2. Using the technical specifications of the sand, we can compute the Trask (or sorting) index S_o and the Hazen (or uniformity) coefficient C_u (Rivière 1977). This calculation requires the quantile q_{25}, q_{60} and q_{75} of the granulometric curve, and gives information on granulometric caracteristics of the sand. We found $S_o = 1.22$ and $C_u = 1.46$ demonstrating that the grain size is very well sorted (monodisperse), resulting in relatively high values of λ.

4.2 Electrokinetic measurements

Streaming potentials are measured between one electrode and the reference (electrode #1, see Figure 1). As for water-content measurements, a time-shift is observed between the beginning of the decrease of each record. Water content measurements were assumed to be integrated over a volume delimited by two consecutive non-polarized electrodes forming a dipole because each water content probe is located in the middle of a dipole. Thus the entire column can be divided into nine different horizontal layers 10 cm high, in which measured streaming potential, measured and computed total water pressure differences and measured water saturations are known as a function of time. Streaming potential differences for each

dipole were inferred from the raw measurements, for the top-five layers in the column. The maximum absolute value of streaming potential is around 7 mV for the first experiment, and almost 45 mV at the end of the second experiment (see Figure 3). Consequently, signals of the first experiment (Figure 3a) are slightly more noisy than those of the second one (Figure 3b). The streaming potential absolute values increase during the drainage, when the water saturation decreases.

We need the total water pressure differences in order to compute the electrokinetic coefficient for each layer inside the column. Total water pressure differences (Figure 4) are inferred for each layer from computed water pressures. Since we showed that the computed values fit the measured values well (Figure 2), computed values of water pressure were preferred over the measured water pressures. The drainage start is characterized by a jump of the computed ΔP. This jump is about 60 Pa for both experiments. After several hours, ΔP inside the layers in the unsaturated part of the column increases. The maximum of ΔP at the end of the experiment depends on the saturation degree in the considered layer; the lower the saturation degree, the higher the ΔP. Thus, $\Delta P_{10,9} \simeq 550$ Pa and $\Delta P_{9,8} \simeq 450$ Pa for the first experiment. Computed ΔP corresponding to layers always located in the saturated part of the column (figure 4) progressively decrease from the start jump to zero.

Using measured streaming potential and computed total water pressure, the following equation leads to electrokinetic coefficient,

$$C = \frac{\Delta V}{\Delta P} \tag{17}$$

Electrokinetic coefficients were computed only in the four layers located in the unsaturated part of the column, i.e $C_{10,9}$, $C_{9,8}$, $C_{8,7}$ and $C_{7,6}$ for the first experiment, and for $C_{10,9}$, $C_{9,8}$, $C_{8,7}$ for the second one. The data from other dipoles (i.e $C_{6,5}$ and lower for exp. 1, and $C_{7,6}$ and lower for exp. 2) were not used because the small values of ΔP gave an unacceptable

signal to noise ratio. The electrokinetic coefficient at saturation was measured during another experiment, and the electrical resistivity was measured at various water contents (see Appendix B).

Obtained values of electrokinetic coefficient are all negative, which involves a negative zeta potential, as expected in sand (Pride & Morgan 1991; Lorne et al. 1999a). The water electrical conductivity and the minimum values of the electrokinetic coefficient observed in each horizontal layer are given in Table 3. These electrokinetic coefficient maximum values (in absolute value) are higher than measured values for similar water conductivities (Ishido & Mizutani 1981; Lorne et al. 1999a) (Figure A6b).

Classically, the minimum value (i.e greatest negative value) of the electrokinetic coefficient is identified in saturated conditions. Measurements of C_{sat} performed on our sand are presented in Appendix B (Figure A6). The values of C_{sat} corresponding to water salinities of experiments #1 and #2 are reported in Table 3. Firstly, the electrokinetic coefficients appear to be not monotonously dependent on water saturation during our drainage experiments (i.e when water saturation decreases) (Figure 5). Secondly, it is clear that the extremum value of the electrokinetic coefficient C_{min}, regardless of the considered dipole, is much greater than the C_{sat} (in absolute value). We also point out that the signals of the first experiment are scattered at the drainage start as shown by a statistical analysis on the uncertainty of the un-normalized measurements (Figure A8). This is why the small values near zero can be either small negative values or small positive values.

5 DISCUSSION

We measured the electrokinetic coefficient for unsaturated conditions to increase for decreasing saturation between 1 and 0.7. These coefficients exceed the C_{sat} value by a factor of ten to two-hundred (Figure 6). This large increase was not

expected and the current models fail to explain this behaviour. Only the electrokinetic coefficient decreasing as S_e decreases (when S_e is below about 0.7) can be adressed by current models, as will be shown below. Our measurements are the first continuous records of the electrokinetic coefficient as a function of water-saturation; thus the proposed power laws (equations 19 and 25 below) that fit the data are not expected to explain the underlying physics but more simply to provide a first basis for empirical models. The exact physical meaning of this increase is not yet understood. Nevertheless, test experiments and uncertainty analysis (Appendix A and B), make no doubt about this result. Thus, the direct effect of the electrical conductivity, which is a crucial parameter for electrokinetics, has been taken into account. Moreover, we do not think that the unexpected electrokinetic coefficient measurements are induced by a special bahaviour of the fluid flow, since we demonstrated that hydrodynamics observations can be classically modeled with the Richards equation. Recently, Jackson (2010) suggested that relative electrokinetic coefficient could be larger than one, but not as much as our measurements. This author proposed that the increase of C_r was linked to the amount of small capillaries fraction in the medium, in the case of a water/oil imbibition flow modelling. However, a direct comparison with this model is not possible since our experiment is a drainage of water within sand.

Even if our observations are larger (in absolute terms) than the calssical measurements, we decided to compare our data to existing models, as their underlying physics could explain a part of our mesurements. However, we cannot use the classical normalization of electrokinetic coefficient to C_{sat} to compare the behaviour of our data and models. Therefore we also normalized the electrokinetic co-

efficient by the minimum value observed during each drainage C_{min} (Figure 7) computed through:

$$C_{norm} = \frac{C(S_w)}{C_{min}} \tag{18}$$

In addition to our dataset, the experimental results of Guichet et al. (2003), performed on sand, are also reported (Figure 7). This comparison shows some consistency of our measurements normalized to the minimum value with existing published values of relative coefficient C_r. As the electrokinetic coefficient values are negative, the normalization by its minimum implies positive values. During the first experiment, when S_w decreases from 1 to 0.8, C_{norm} in the four unsaturated layers increases. Then, for ${S_w}^{min} < S_w < 0.8$, C_{norm} monotonously decreases. The parameter ${S_w}^{min}$ is introduced here to characterize the minimum of the measured water saturation. It is preferred to ${S_w}^r$, since ${S_w}^r$ is a parameter which clearly depends on experimental conditions, like applied ΔP or temperature for instance. Thus, in the conditions of our experiments, there was no flow for $S_w < 0.35$ ($\equiv S_e < 0.08$) and for $S_w < 0.4$ ($\equiv S_e < 0.11$) for the first and the second drainage respectively. For the second experiment (Figure 7b), C_{norm} increases when S_w decreases from 1 to about 0.95 considering the dipole $(8, 7)$ and from 1 to 0.8 for the dipole $(9, 8)$. The value of C_{norm} for the dipole $(10, 9)$ is maximum when S_w is around 0.65. The slope of the increasing part of this signal (for $0.55 < S_w < 1$) is smaller than for the two other dipoles. Therefore, a shift from $\simeq 15\%$ to $\simeq 20\%$ (for $C_{10,9}$ of exp. #2) of the maximum location is observed between the two experiments, however both experiments describe a similar behaviour of $C(S_w)$ in the whole range of water saturation. Thus, one can conclude that the electrokinetic coefficient does not depend monotonously on the water-content, either linearly nor as a power-law, as suggested by previous studies. The maximum of the normalized electrokinetic coefficient is located between 0.65 and 0.95 of water saturation. This complex behaviour of the electrokinetic co-

efficient has never before been reported, especially the large increase for $0.8 - 0.95 < S_w < 1$ (excluding $C_{10,9}$ of the second experiment), and is a very important result for the understanding of electrokinetic phenomena in unsaturated media.

We compare our measurements, normalized using equation 18, to the four C_r models introduced in Section 2 by equations 12, 13 and 15 (Figure 8). Hydraulic parameter λ deduced from our modelling of water-flow (Table 2) and $L = 0.5$ were used in equation 7, to compute equation 14. In addition, a modified model from Perrier & Morat (2000) is also computed using ${S_w}^r$ from the inversion process, instead of the value 0.1 for ${S_w}^r$ they used in their k_r model (equation 13). Futhermore, the saturation Archie exponent n needed to compute these models is deduced from electrical resistivity measurements carried out on a small-scale column (used for Theta probe calibration), and its value is $n = 1.45$ (see Appendix B for details). These models describe a uniform decrease of the normalized electrokinetic coefficient as water saturation decreases. Moreover, their common feature is that C_{sat} is the maximum value of the electrokinetic coefficient. Although these models depend on a combination of S_e or S_w, we compared them to a power law of the effective water saturation. The Guichet et al. (2003), Saunders et al. (2008) and the Perrier & Morat (2000) models show a convex curvature. Comparing these three models to a law of the form ${S_e}^\beta$ leads to β equal to 1, 0.5 and $\simeq 0.8$ respectively. By contrast, the Revil et al. (2007) and the modified Perrier & Morat (2000) models show a concave curvature. The same comparison to a power law would lead to exponents around 1.55 and 1.2 respectively. It seems that our dataset, when ${S_e}^{min} < S_e < 1$, would be better fitted by a model with a convex curvature, which corresponds to an exponent β less or close to 1. One can conclude that our dataset cannot be **explained by existing models in the whole range of saturation**, because of the presence of two different behaviours of the electrokinetic coefficient, in two water saturation domains.

In order to model the behaviours of C_{norm} for ${S_e}^{min} < S_e < 0.7 - 0.9$ and for $0.7 - 0.9 < S_e < 1$, we propose to fit our measurements by an empirical law introduced by equation 19. These two domains exclude the dipole $C_{10,9}$ of the second experiment (with the maximum value of C_{norm} located at $S_e = 0.55$), which will be considered apart.

$$\frac{C(S_w)}{C_{min}} = \alpha \left(\frac{\theta - \theta_r}{\theta_s - \theta_r} \right)^{\beta} = \alpha {S_e}^{\beta} \tag{19}$$

where α and β are adjusted parameters [-] and S_e is the effective water saturation. This empirical law, based on our continuous records, is an alternative law which can be used when the behaviour of the electrokinetic coefficient as a function of water saturation is necessary.

The equation 19 was fitted (Figure 9) in a least-square sense to electrokinetic coefficient data. A constraint was used to force $max(C_{norm}) \simeq 1$, within a tolerance of 10%. The fit of equation 19 was performed independently for ${S_e}^{min} < S_e < 0.7 - 0.9$ and for $0.7 - 0.9 < S_e < 1$, except for the dipole $C^2_{10,9}$ for which the equation was fitted for ${S_e}^{min} < S_e < 0.55$, $0.55 < S_e < 0.9$ and in the whole saturation domain (${S_e}^{min} < S_e < 0.9$). The dipole $C_{8,7}$ of the second experiment was not fitted for $0.9 < S_e < 1$, because less than ten points were available in this part where water saturation decreases very fast. We first consider all the dipoles except $C_{10,9}$ for the second experiment. Computed values of α and β are reported in Table 4. These values show that a power law from ${S_e}^{0.32}$ to ${S_e}^{1.22}$ for ${S_e}^{min} < S_e < 0.7 - 0.9$ fits the data, depending on the chosen dipole (Figure 9). Saunders et al. (2008) suggested that this exponent could vary between 0.01 and 1, which is consistent with our results in the domain ${S_e}^{min} < S_e < 0.55 - 0.9$. The fit of the equation 19 in the range $0.7 - 0.85 < S_e < 1$ leads to negative values of β. We deduce that β can varies from -8.5 to -0.58. The dipole $C_{10,9}$ of the second experiment shows some different behaviour, so that exponent β was adjusted three times, for ${S_e}^{min} < S_e < 0.55$, for $0.55 < S_e < 0.9$ and in the whole range

of saturation. Adjusted values of β are then 0.65, -0.26 and 0.25 respectively. Thus, the widest range of β would be from -8.5 to -0.26 for $0.55 - 0.9 < S_e < 1$ and from 0.32 to 1.22 for ${S_e}^{min} < S_e < 0.55 - 0.9$. Moreover, we can conclude that the exponent β is less or very close to 1. Thus, an empirical law based on all signals, is here proposed to characterize the behaviour of the electrokinetic coefficient in unsaturated conditions:

$$C_{norm} = \alpha {S_e}^{\beta}$$

$$\text{with} \begin{cases} -8.5 < \beta < -0.26, \text{ for } 0.55 - 0.9 < S_e < 1 \\ 0.32 < \beta < 1.22, \text{ for } {S_e}^{min} < S_e < 0.55 - 0.9 \end{cases} \tag{20}$$

The $C^1_{10,9}$ signal shows a distinct maximum as a function of saturation (see Figure 9a), whereas the one for $C^2_{10,9}$ is less marked. However, the dipole $(10, 9)$ seems to have a particular behaviour in both experiments compared to other dipoles in terms of fitted β, so that it will be considered independently in the next part of this work.

We concluded previously that both Perrier & Morat (2000) and Revil et al. (2007) models could not fit our measurements using the equations 13 and 14. We propose to modify these two relations by introducing a new parameter that we can call the electrokinetic residual saturation, written $S_w^{r,ek}$. This parameter corresponds to the water saturation at which electrokinetic coupling stops. We consider that the residual water saturation ${S_w}^r$, classically used in hydrodynamics to characterize the volume of adsorbed water in unsaturated conditions, is different from $S_w^{r,ek}$. Using this concept, let us write again two relations based on equations 13 and 14 to describe the normalized electrokinetic coefficient:

$$C_{norm,1} = \frac{\Gamma_{w,1}}{{S_w}^n} \tag{21}$$

$$C_{norm,2} = \frac{\Gamma_{w,2}}{{S_w}^{n+1}} \tag{22}$$

where $\Gamma_{w,1}$ and $\Gamma_{w,2}$ are deduced by analogy to relative permeability models. $\Gamma_{w,1}$ is defined

by,

$$\Gamma_{w,1} = \left(\frac{S_e - S_w^{r,ek}}{1 - S_w^{r,ek}} \right)^2 = {S_{ek}}^2 \tag{23}$$

and $\Gamma_{w,2}$ by,

$$\Gamma_{w,2} = \left(\frac{S_e - S_w^{r,ek}}{1 - S_w^{r,ek}} \right)^{L+2+\frac{2}{\lambda}} = {S_{ek}}^{L+2+\frac{2}{\lambda}} \tag{24}$$

with S_{ek} the electrokinetic water saturation. The functions $\Gamma_{w,1}$ and $\Gamma_{w,2}$ are very close to those in Adler et al. (1997) and Mualem (1976a) respectively. We also propose the following relationship, which is modified from the equation 19,

$$C_{norm} = \left(\frac{S_e - S_w^{r,ek}}{1 - S_w^{r,ek}} \right)^{\beta_{ek}} = {S_{ek}}^{\beta_{ek}} \tag{25}$$

We used equations 21, 22 and 25 to fit four electrokinetic coefficient curves from the two experiments presented in this work, $C^1_{9,8}$, $C^1_{8,7}$, $C^2_{9,8}$ and $C^2_{8,7}$. These relations are fitted in a least-square sense with $S_w^{r,ek}$ adjusted but constrained to be positive. The parameter β_{ek} of the equation 25 is also adjusted. The results of this calculation are shown in Figures 10b, d and f. As it was noticed before, the dipoles $C^1_{10,9}$ and $C^2_{10,9}$ were considered independently (Figures 10a, c and e). In the same way than for equation 19, the equations 21, 22 and 25 were fitted to $C^2_{10,9}$ in the whole range of saturation, and for ${S_e}^{min} < S_e < 0.55$ independently. The values of $S_w^{r,ek}$ (Table 5) are smaller than ${S_w}^r$ values (Table 2). The fitted $S_w^{r,ek}$ from equations 21 and 22 are very similar only for a given dipole. These two models are extremely dependent on the chosen $\Gamma_{w,i}$ (particularly on the power exponent) and on Archie's saturation exponent n, which is involved in the behaviour of the unsaturated electrical conductivity. Indeed, the numerator and the denominator exponents balance each other. These models are roughly equivalent, leading to similar values of ${S_w}^{r,ek}$. Moreover, these two models seem to have not enough degrees of freedom to fit data from dipoles $C^1_{10,9}$ and $C^2_{10,9}$. The third model fit (equation 25) gives some higher and very homogeneous values

of $S_w^{r,ek}$, around 0.13 for dipoles $C_{9,8}^1$, $C_{8,7}^1$, $C_{9,8}^2$ and $C_{8,7}^2$, and around 0.09 for dipoles $C_{10,9}^1$ and $C_{10,9}^2$. Values of β_{ek} are also very homogeneous from a dipole to another. The results gives $\beta_{ek} \simeq 0.2$ for $C_{10,9}^1$ and $C_{10,9}^2$, and $0.4 < \beta_{ek} < 0.6$ for $C_{9,8}^1$, $C_{8,7}^1$, $C_{9,8}^2$ and $C_{8,7}^2$. These coherent values for both parameters $S_w^{r,ek}$ and β_{ek} lead to the conclusion that the model we propose through equation 25 is more appropriate than the models given by equation 21 and 22.

In order to roughly estimate the thickness of the adsorbed water layer corresponding to the electrokinetic residual saturation, we propose to use the method described by Knight (1991) to compute the equivalent number of monolayers of water. This method uses the assumption that all the water is present as a layer with constant thickness and that covers all the surface area of pores. Although the interface is composed of an EDL rather than monolayers in saturated conditions (Revil & Glover 1997), this approach gives the possibility to roughly estimate the thickness of the adsorbed layer expected at different electrokinetic residual saturation $S_w^{r,ek}$. We estimated the internal surface area of the sand, from its technical specifications, to be 11.3 $m^2.kg^{-1}$. Taking 0.35 nm as the thickness of a monolayer of water (Thorp 1959), we computed the equivalent number of monolayers of water (Table 5) corresponding to the fitted values of $S_w^{r,ek}$. These values constitute the thickness of the adsorbed water at the grain surface. The equivalent numbers of monolayers inferred from adjusted $S_w^{r,ek}$ of the table 5 for equation 25, vary from 2.4 to 3.74, which corresponds to thickness from 0.84 nm to 1.31 nm. One monolayer of water would correspond to electrokinetic residual saturation of 0.04, which could be considered as a minimumvalue of ${S_w}^{r,ek}$. On the other hand, Knight (1991) considered that a thickness of 0.5 monolayer of water is possible. This would lead to a minimum value of ${S_w}^{r,ek}$ of 0.02. Physically, the introduction of $S_w^{r,ek}$ involves the possibility of electrokinetics to appear while water flow is too small to be measured. Therefore the electrokinetics occuring at such low saturations appear within the residual water.

Then, considering the electrical double layer model in the "thin double layer approximation" (or Debye approximation), we computed the so-called Debye length, which is a measure of the diffuse double layer thickness,

$$\chi = \sqrt{\frac{\epsilon k_B T}{e^2 C}} \tag{26}$$

where k_B is the bolztmann's constant, T is the temperature in Kelvin, e is the elementary charge [C] and C is the concentration equivalent to the ions per unit of volume deduced from electrical conductivity measurements. For measured $\sigma_w = 103.2 \times 10^{-4}$ S.m^{-1} (first experiment) and $\sigma_w = 66.4 \times 10^{-4}$ S.m^{-1} (second experiment), we computed $\chi \simeq 15$ nm. These values are in good agreement with the values published in the literature for such electrolyte concentrations (Pride 1994).

We point out that the values of the electrokinetic residual saturation deduced from our experiments are ranging between 0.09 and 0.13 (using equation 25). The thickness of adsorbed water layer corresponding to ${S_w}^{r,ek}$ is about 1 nm, which is below the electrical double layer thickness in saturated state of $\simeq 15$ nm.

6 CONCLUSIONS

An unexpected behaviour of the electrokinetic coefficient has been presented in this work. Indeed, it has been shown that the normalized electrokinetic coefficient increases and then decreases when water saturation decreases during a drainage, with a maximum of $C(S_w)/C_{min}$ for $S_w = 0.65 - 0.8$. We have demonstrated by using inverse hydraulic parameters, that existing models could not explain this complex behaviour. We propose first that an empirical power law, as $\alpha {S_e}^{\beta}$, could model electrokinetic coefficient data. Moreover, we introduce the concept of the electrokinetic residual saturation $S_w^{r,ek}$. Using this parameter, and although only this parameter is adjusted, it allows us to better fit our dataset and to propose a new

model (eq.25). We show that the values of ${S_w}^{r,ek}$ are roughly 0.1, which would correspond to a thickness of adsorbed water of about 1 nm. Most of the values of the β_{ek} exponent are in the range $0.4 - 0.6$ for saturation up to 0.8. Other drainage experiments are needed to confirm the model that we propose. Streaming potential and hydrodynamic measurements should be jointly inverted, taking into account electrical conductivity variations, in order to deduce a robust law of the electrokinetic coefficient behaviour in unsaturated conditions. **Further experiments should help to propose alternative models and possible explanations for the underlying physical processes. It involves drainage experiments with different hydrodynamic conditions. The comparison between drainage and imbibition experiments should give some pieces of explanations**.

7 ACKNOWLEDGMENTS

This work was supported by the French National Scientific Center (CNRS), by ANR-TRANSEK, and by REALISE the "Alsace Region Research Network in Environmental Sciences in Engineering" and the Alsace Region. We thank P. W. Glover and an anonymous reviewer for their very constructive reviews. The authors would like to thank M. Pierre-Daniel Matthey for his usefull advises during the experiment conception, and M. Julien Allègre for his contribution in the numerical design of the experimental setup.

REFERENCES

Adler, P. M., Thovert, J.-F., Jacquin, C., Morat, P., & Moul, J.-L. L., 1997. Electrical signals induced by the atmospheric pressure variations in unsaturated media, *C.R. Acad. Sci. Paris, serie IIa*, **324**, 711–718.

Ahmad, M. U., 1964. A laboratory study of streaming potentials, *Geophysical Prospecting*, **12**, 49–64.

Archie, G. E., 1942. The electrical resistivity log as an aid in determining some reservoir characteristics, *Trans. Am. Inst. Min. Metall. Pet. Eng.*, pp. 146–154.

Bogolovsky, V. A. & Ogilvy, A. A., 1970. Natural potential anomalies as a quantitive index of the rate of seepage from water reservoirs, *Geophysical Prospecting*, **18**, 261–268.

Bordes, C., Jouniaux, L., Dietrich, M., Pozzi, J.-P., & Garambois, S., 2006. First laboratory measurements of seismo-magnetic conversions in fluid-filled fontainebleau sand, *Geophys. Res. Lett.*, **33**, L01302.

Bordes, C., Jouniaux, L., Garambois, S., Dietrich, M., Pozzi, J.-P., & Gaffet, S., 2008. Evidence of the theoretically predicted seismo-magnetic conversion, *Geophys. J. Int.*, **174**, 489–504.

Brooks, R. J. & Corey, A. T., 1964. Hydraulic properties of porous media, *Hydrol. Pap.*, **3**, 318–333.

Carsel, R. F. & Parrish, R. S., 1988. Developing joint probability distributions of soil water retention characteristics, *Water Resour. Res.*, **24**(5), 755–769.

Corey, A. T., 2002. *Simultaneous determination of water transmission and retention properties. Direct Methods. IN: Methods of Soil Analysis. Part 4. Physical Methods. (J.H. Dane and G.C. Topp, Eds.)*, vol. 5, Soil Science Society of America Book Series.

Darnet, M. & Marquis, G., 2004. Modelling streaming potential (sp) signals induced by water movement in the vadose zone, *Journal of Hydroloy*, **285**, 114–124.

Darnet, M., Marquis, G., & Sailhac, P., 2003. Estimating aquifer hydraulic properties from the inversion of surface streaming potential (sp) anomalies, *Geophys. Res. Lett.*, **30**, 1679.

Darnet, M., G.Marquis, & Sailhac, P., 2006. Hydraulic stimulation of geothermal reservoirs:fluid flow, electric potential and microseismicity relationships, *Geophys. J. Int.*, **166**, 438–444.

Davis, J. A., James, R. O., & Leckie, J., 1978. Surface ionization and complexation at the oxide/water interface, *Journal of Colloid and Interface Science*, **63**, 480–499.

Doussan, C., Jouniaux, L., & Thony, J.-L., 2002. Variations of self-potential and unsaturated flow with time in sandy loam and clay loam soils, *Journal of Hydrology*, **267**, 173–185.

Dukhin, S. S. & Derjaguin, B. V., 1974. *Surface and Colloid Science, edited by E. Matijevic*, John Wiley and sons, New York.

Finizola, A., Sortino, F., Lenat, J.-F., & Valenza, M., 2002. Fluid circulation at stromboli volcano (aeolian islands, italy) from self potential and co2 surveys, *J. Volc. Geotherm. Res.*, **116**, 1–18.

Finizola, A., Lenat, J.-F., Macedo, O., Ramos, D., Thouret, J.-C., & Sortino, F., 2004. Fluid

circulation and structural discontinuities inside misti volcano (peru) inferred from sel-potential measurements, *J. Volc. Geotherm. Res.*, **135**(4), 343–360.

Garambois, S. & Dietrich, M., 2001. Seismoelectric wave conversions in porous media: Field measurements and transfer function analysis., *Geophysics*, **66**, 1417–1430.

Garambois, S. & Dietrich, M., 2002. Full waveform numerical simulations of seismoelectromagnetic wave conversions in fluid-saturated stratified porous media., *J. Geophys. Res.*, **107**(B7), ESE 5–1–ESE 5–18.

Gaskin, G. J. & Miller, J. D., 1996. Measurement of soil water content using a simplified impedance measuring technique, *Journal of Agricultural Engineering Research*, **63**, 153–160.

Gibert, D. & Pessel, M., 2001. Identification of sources of potential fields with the continuous wavelet transform: application to self-potential profiles, *Geophys. Res. Lett.*, **28**, 1863–1866.

Glover, P. W. J. & Walker, E., 2009. Grain-size to effective pore-size transformation derived from electrokinetic theory, *Geophysics*, **74**, E17–E29.

Glover, P. W. J., Zadjali, I. I., & Frew, K. A., 2006. Permeability prediction from micp and nmr data using an electrokinetic approach, *Geophysics*, **71**, F49–F60.

Guichet, X., Jouniaux, L., & Pozzi, J.-P., 2003. Streaming potential of a sand column in partial saturation conditions, *J. Geophys. Res.*, **108**(B3), 2141.

Guichet, X., Jouniaux, L., & Catel, N., 2006. Modification of streaming potential by precipitation of calcite in a sand-water system: laboratory measurements in the ph range from 4 to 12, *Geophys. J. Int.*, **166**, 445–460.

Hase, H., Ishido, T., Takakura, S., Hashimoto, T., Sato, K., & Tanaka, Y., 2003. Zeta potential measurement of volcanic rocks from aso caldera, *Geophys. Res. Lett.*, **23**(30), 2210.

Haverkamp, R., Zammit, C., Bouraoui, F., Rajkai, K., Arrúe, J., & Heckmann, N., 1998. Grizzly, grenoble catalogue of soils: Survey of soil field data and description of particle-size, soil water retention and hydraulic conductivity functions. laboratoire d'etude des transferts en hydrologie et environnement (lthe), grenoble, cedex 9, france, *Pers. Comm.*.

Haverkamp, R., Leij, F. J., Fuentes, C., Sciortino, A., & Ross, P. J., 2005. Soil water retention: I. introduction of a shape index, *Soil Sci. Soc. Am. J.*, **69**, 18811890.

Hayek, M., Lehmann, F., & Ackerer, P., 2007. Adaptative multi-scale parametrization for one-dimensional flow in unsaturated porous media, *Adv. Water Resour.*.

Henry, P., Jouniaux, L., Screaton, E. J., Hunze, S., & Saffer, D. M., 2003. Anisotropy of electrical

conductivity record of initial strain at the toe of the nankai accretionary wedge, *J. Geophys. Res.*, **108**(B9), ETG 2–1–ETG 2–12.

Hopmans, J., Simunek, J., Romano, N., & Durner, W., 2002. *Simultaneous determination of water transmission and retention properties. Direct Methods. IN: Methods of Soil Analysis. Part 4. Physical Methods. (J.H. Dane and G.C. Topp, Eds.)*, vol. 5, Soil Science Society of America Book Series.

Ishido, T., 2004. Electrokinetic mechanism for the w-shaped self-potential profile on volcanoies, *Geophys. Res. Lett.*, **31**, L15616.

Ishido, T. & Mizutani, H., 1981. Experimental and theoretical basis of electrokinetic phenomena in rock water systems and its applications to geophysics, *J. Geophys. Res.*, **86**, 1763–1775.

Jaafar, M. Z., Vinogradov, J., & Jackson, M. D., 2009. Measurement of streaming potential coupling coefficient in sandstones saturated with high salinity nacl brine, *Geophys. Res. Lett.*, **36**, L21306.

Jackson, M. D., 2008. Characterization of multiphase electrokinetic coupling using a bundle of capillary tubes model, *J. Geophys. Res.*, **113**, B04201.

Jackson, M. D., 2010. Multiphase electrokinetic coupling: Insights into the impact of fluid and charge distribution at the pore-scale from a bundle of capillary tubes model, *J. Geophys. Res.*, p. in press.

Jouniaux, L. & Pozzi, J.-P., 1997. Laboratory measurements anomalous 0.1-0.5 hz streaming potential under geochemical changes: Implications for electrotelluric precursors to earthquakes, *J. Geophys. Res.*, **102**, 15,335–15,343.

Jouniaux, L., Lallemant, S., & Pozzi, J., 1994. Changes in the permeability, streaming potential and resistivity of a claystone from the nankai prism under stress, *Geophys. Res. Lett.*, **21**, 149–152.

Jouniaux, L., Pozzi, J.-P., Berthier, J., & Massé, P., 1999. Detection of fluid flow variations at the nankai trough by electric and magnetic measurements in boreholes or at the seafloor, *J. Geophys. Res.*, **104**, 29293–29309.

Jouniaux, L., Bernard, M.-L., Zamora, M., & Pozzi, J.-P., 2000. Streaming potential in volcanic rocks from mount peleé, *J. Geophys. Res.*, **105**, 8391–8401.

Knight, R., 1991. Hysteresis in the electrical resistivity of partially saturated sandstones, *Geophysics*, **56**(12), 2139–2147.

Lehmann, F. & Ackerer, P., 1998. Comparison of iterative methods for omproved solutions of the fluid flow equation inpartially saturated porous media, *Transport in Porous media*, **31**, 275–292.

Leij, F. J., Haverkamp, R., Fuentes, C., Zatarain, F., & Ross, P. J., 2005. Soil water retention: Ii. derivation and application of shape index, *Soil Sci. Soc. Am. J.*, **69**, 18911901.

Lesmes, D. P. & Friedman, S. P., 2006. *Relationships between the electrical and hydrogeological properties of rocks and soils*, Y Rubin and S Hubbard, Springer, in Hydrogeophysics.

Li, S. X., Pengra, D. B., & Wong, P., 1995. Onsager's reciprocal relation and the hydraulic permeability of porous media, *J. Geophys. Res.*, **51**(6), 5748–5751.

Linde, N., Jougnot, D., Revil, A., Matthai, S. K., Renard, D., & Doussan, C., 2007. Streaming current generation in two-phase flow conditions, *Geophys. Res. Lett.*, **34**, LO3306.

Lorne, B., Perrier, F., & Avouac, J.-P., 1999a. Streaming potential measurements. 1. properties of the electrical double layer from crushed rock samples, *J. Geophys. Res.*, **104**(B8), 17.857–17.877.

Maineult, A., Bernabé, Y., & Ackerer, P., 2004. Electrical response of flow, diffusion and advection in a laboratory sand box, *Vadose Zone J.*, **3**, 1180–1192.

Maineult, A., Bernabé, Y., & Ackerer, P., 2005. Detection of advected concentration and ph fronts from self-potential measurements, *J. Geophys. Res.*, **110**, B11205.

Maineult, A., Strobach, E., & Renner, J., 2008. Self-potential signals induced by periodic pumping test, *J. Geophys. Res.*, **113**, B01203.

Marquis, G., Darnet, M., Sailhac, P., Singh, A. K., & Gérard, A., 2002. Surface electric variations induced by deep hydraulic stimulation: an example from the soultz hdr site, *Geophys. Res. Lett.*, **29**.

Marshall, D. J. & Madden, T. R., 1959. Induced polarization, a study of its causes, *Geophysics*, **24**(4), 790–816.

Massenet, F. & Pham, V. N., 1985. Experimental and theoretical basis of self-potential phenomena in volcanic areas with reference to results obtained on mount etna, *Earth and Planetary Science Letters*, **73**, 415–429.

Morgan, F. D., Williams, E. R., & Madden, T. R., 1989. Streaming potential properties of westerly granite with applications, *J. Geophys. Res.*, **94**(B9), 12.449–12.461.

Mualem, Y., 1976a. A new model for predicting the hydraulic conductivity of unsaturated porous media, *Water Resour. Res.*, **12**, 513–522.

Naudet, V., Revil, A., Bottero, J.-Y., & Bégassat, P., 2003. Relationship between self-potential

(sp) signals and redox conditions in contaminated groundwater, *Geophys. Res. Lett.*, **30**(21), HLS 2–1–HLS 2–4.

Onizawa, S., Matsushima, N., Ishido, T., Hase, H., Takakura, S., & Nishi, Y., 2009. Self-potential distribution on active volcano controlled by three-dimensional resistivity structure in izu-oshima, japan, *Geophys. J. Int.*, **178**, 1164–1181.

Onsager, L., 1931. Reciprocical relation in irreversible processes: I, *Phys. Rev*, **37**.

Overbeek, J. T. G., 1952. Electrochemistry of the double layer., *Colloid Science, Irreversible Systems, edited by H. R. Kruyt, Elsevier*, **1**, 115–193.

Pengra, D. B., Li, S. X., & Wong, P., 1999. Determination of rock properties by low frequency ac electrokinetics, *J. Geophys. Res.*, **104**(B12), 29485–29508.

Perrier, F. & Froidefond, T., 2003. Electrical conductivity ans streaming potential coefficient in a moderately alkaline lava series, *Earth and Planetary Science Letters*, **210**, 351–363.

Perrier, F. & Morat, P., 2000. Characterization of electrical daily variations induced by capillary flow in the non-saturated zone, *Pure and Appl. Geophys*, **157**, 785–810.

Pezard, P., Gautier, S., Borgne, T. L., Legros, B., & Deltombe, J.-L., 2009. Muset: A multiparameter and high precision sensor for downhole spontaneous electrical potential measurements, *Comptes Rendus - Geoscience*, **341**, 957–964.

Pinder, G. F. & Gray, W. G., 1977. Finite element simulation in surface and subsurface hydrology, *New York: Academic Press*.

Pozzi, J.-P. & Jouniaux, L., 1994. Electrical effects of fluid circulation in sediments and seismic prediction, *C.R. Acad. Sci. Paris, serie II*, **318**(1), 73–77.

Pride, S., 1994. Governing equations for the coupled electromagnetics and acoustics of porous media, *Physical Review B*, **50**, 15678–15695.

Pride, S. & Morgan, F. D., 1991. Electrokinetic dissipation induced by seismic waves, *Geophysics*, **56**(7), 914–925.

Rawls, W. J., Brakensiek, D. L., & Saxton, K. E., 1982. Estimation of soil water properties, *Trans. ASAE*, **25**, 1316–1320.

Revil, A. & Glover, P. W., 1997. Theory of ionic-surface electrical conduction in porous media, *Physical Review B*, **55**(3), 1757–1773.

Revil, A., Pezard, P. A., & Glover, P. W. J., 1999a. Streaming potential in porous media: 1. theory of the zeta potential., *J. Geophys. Res.*, **104**(B9), 20.021–20.031.

Revil, A., Linde, N., Cerepi, A., Jougnot, D., Matthai, S., & Finsterle, S., 2007. Electrokinetic coupling in unsaturated porous media, *Journal of Colloid and Interface Science*, **313**, 315–327.

Richards, L. A., 1931. Capillary conduction of liquids through porous medium, *Physics*, **1**, 318–333.

Rivière, A., 1977. *Méthodes granulométriques: Techniques et interprtations*, Masson, Paris.

Sailhac, P. & Marquis, G., 2001. Analytic potentials for the forward and inverse modeling of sp anomalies caused by subsurface fluid flow, *Geophys. Res. Lett.*, **28**, 1851–1854.

Sailhac, P., Darnet, M., & Marquis, G., 2004. Electrical streaming potential measured at the ground surface: forward modeling and inversion issues for monitoring infiltration and characterizing the vadose zone, *Vadose Zone J.*, **3**, 1200–1206.

Saunders, J. H., Jackson, M. D., & Pain, C. C., 2008. Fluid flow monitoring in oilfields using downhole measurements of electrokinetic potential, *Geophysics*, **73**, E165E180.

Schön, J., 1996. *Physical properties of rocks - fundamentals and principles of petrophysics*, vol. 18, Elsevier Science Ltd., Handbook of Geophysical Exploration, Seismic exploration.

Smoluchowski, M., 1905. Zur theorie der elektrischen kataphorese und der oberflchenleitung, *Physikalische Z*, **6**, 529–536.

Sprunt, E. S., M., T. B., & Djabbarah, N. F., 1994. Streaming potential from multiphase flow, *Geophysics*, **59**(5), 707–711.

Stern, O., 1924. Zur theorie der electrolytischen doppelschicht, *Z. Electrochem.*, (30), 508–516.

Strahser, M. H., Rabbel, W., & Schildknecht, F., 2007. Polarisation and slowness of seismoelectric signals: a case study, *Near Surface Geophysics*, **5**, 97–114.

Thorp, J. M., 1959. The dielectric behaviour of vapors adsorbed on porous solids, *Trans. Faraday. Soc.*, **55**, 442.

Titov, K., Revil, A., Konosavsky, P., Straface, S., & Troisi, S., 2005. Numerical modelling of self-potential signals associated with a pumping test experiment, *Geophys. J. Int.*, **162**, 641–650.

Tosha, T., Matsushima, N., & Ishido, T., 2003. Zeta potential measured for an intact granite sample at temperatures to 200c, *Geophys. Res. Lett.*, **30**(6), 1295.

Table 1. Petrophysical characteristics of the sand used in the experimental setup.

ϕ [-]	grains size [μm]	q_{25}, q_{60}, q_{75} [μm]	SiO_2 [%]	Others components [%]
0.36-0.37	100-300	247, 220, 165	> 99.7	< 0.3

Table 2. Hydrodynamic parameters values deduced from the inversion process for the two experiments. ${S_w}^r$ values are deduced from θ_r through ${S_w}^r = \theta_r/\phi$. K_s^{meas} is the measured permeability of our sand. The saturation Archie exponent is measured $n = 1.45$

Experiment	K_s (x10^{-5}) [m.s^{-1}]	K_s^{meas} (x10^{-5}) [m.s^{-1}]	h_a [m]	λ	θ_r	θ_s [m^3.m^{-3}]	${S_w}^r$ [-]
1	1.65	17.2	0.4	3.88	0.11	0.355	0.305
2	2.72	17.2	0.45	3.65	0.12	0.358	0.33

Table 3. Minimum values of C(S_w) in the three/four unsaturated layers and saturated values C_{sat}, for both experiments. The water electrical conductivity was measured at the end of each drainage. The equilibrium phase is detailed in A.

Exp #1		Exp #2	
Dipole	C_{min} [V.Pa^{-1}]	Dipole	C_{min} [V.Pa^{-1}]
$10, 9$	-1.67x10^{-5}	$10, 9$	-6.7x10^{-5}
$9, 8$	-2.04x10^{-5}	$9, 8$	-2.7x10^{-4}
$8, 7$	-4.8x10^{-5}	$8, 7$	-5.9x10^{-4}
$7, 6$	-5.3x10^{-5}	/	/
σ_w(x10^{-4}) [S.m^{-1}]		σ_w(x10^{-4}) [S.m^{-1}]	
103.2		66.4	
C_{sat} [V.Pa^{-1}]		C_{sat} [V.Pa^{-1}]	
-1.6x10^{-6}		-2.5x10^{-6}	

Table 4. Equation 19) fitted parameters in both the decreasing and the increasing phase of the electrokinetic coefficient of the two experiments. Exponents 1 and 2 mean first and second experiment respectively.

	$S^{min} < S_e < 0.7 - 0.85$		$0.7 - 0.85 < S_e < 1$	
Dipole	α [-]	β [-]	α [-]	β [-]
$C^1_{10,9}$	1.04	0.32	0.07	-8.5
$C^1_{9,8}$	1.51	1.22	0.45	-2.6
$C^1_{8,7}$	1.42	0.97	0.62	-1.19
$C^1_{7,6}$	1.14	0.49	0.91	-0.58
$C^2_{10,9}$	1.64	0.65	0.85	-0.26
$C^2_{9,8}$	1.38	1.21	0.56	-1.69
$C^2_{8,7}$	0.96	0.75	/	/
	$S^{min} < S_e < 0.9$			
$C^2_{10,9}$	0.26			

Table 5. Fitted parameters of equations 21, 22 and 25 compared to our dataset. The value $n = 1.45$ is used for the Archie saturation exponent.

	eq. 21	eq. 22	eq. 25	
	$S_w^{r,ek}$	$S_w^{r,ek}$	$S_w^{r,ek}$	β_{ek}
$C^1_{10,9}$	/	/	0.088	0.24
$C^1_{9,8}$	0.064	0.04	0.13	0.55
$C^1_{8,7}$	0.019	0.011	0.13	0.42
$C^2_{10,9}$	/	/	0.09	0.18
$C^2_{9,8}$	0.059	0.57	0.12	0.57
$C^2_{8,7}$	0.05	0.053	0.11	0.53
	number of monolayers			
$C^1_{10,9}$	/	/	2.4	
$C^1_{9,8}$	1.73	1.08	3.74	
$C^1_{8,7}$	0.51	0.3	3.59	
$C^2_{10,9}$	/	/	2.5	
$C^2_{9,8}$	1.62	1.57	3.39	
$C^2_{8,7}$	1.37	1.46	3.17	

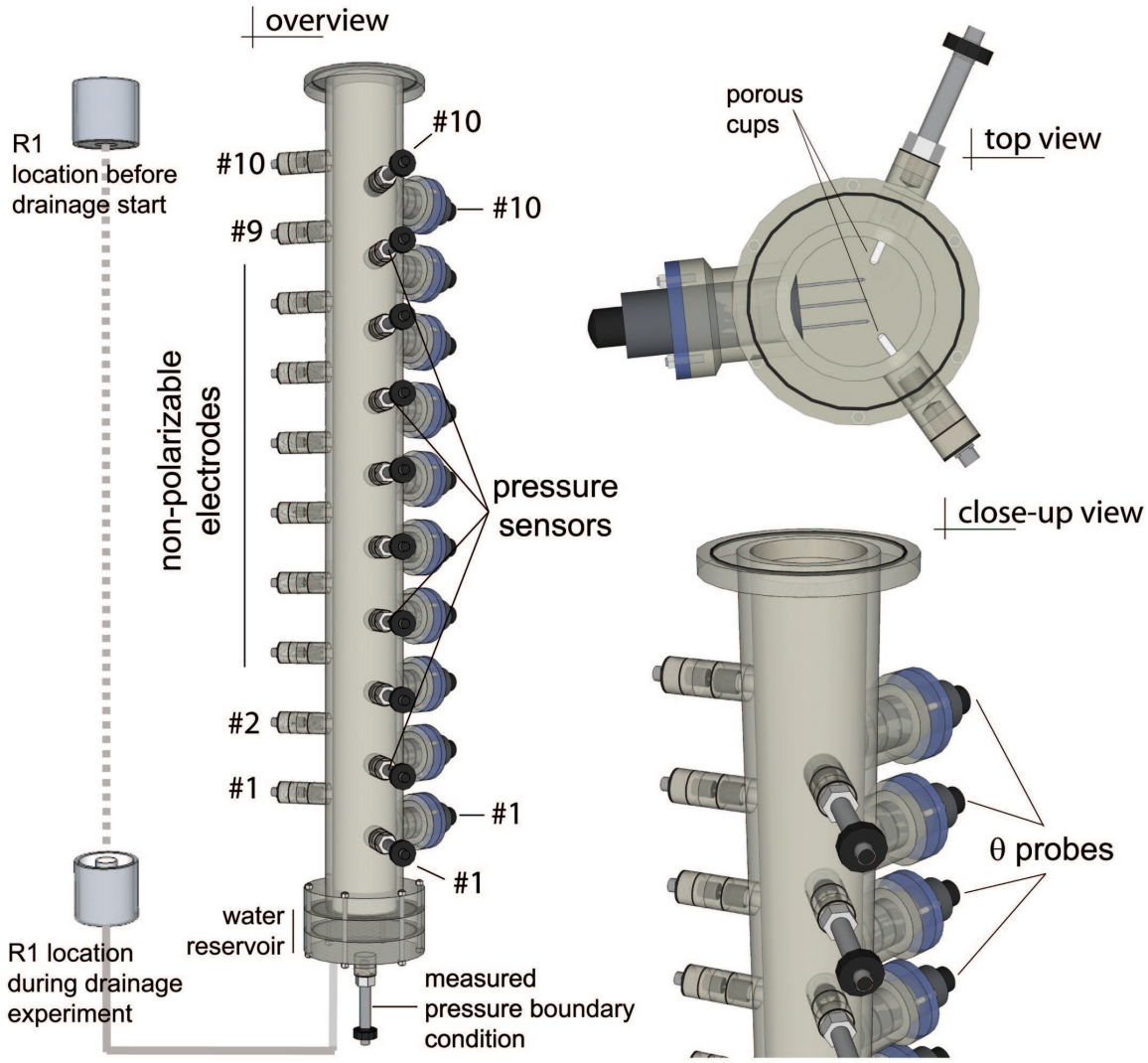

Figure 1. Sketch of the experimental setup. The plexiglas column is 10 cm diameter and 1.3 meter height. Ten non polarizable electrodes are located every 10 cm along the column. The water reservoir R1 is used to apply the pressure condition at the bottom of the column. A pressure sensor monitors this boundary condition during the experiment.

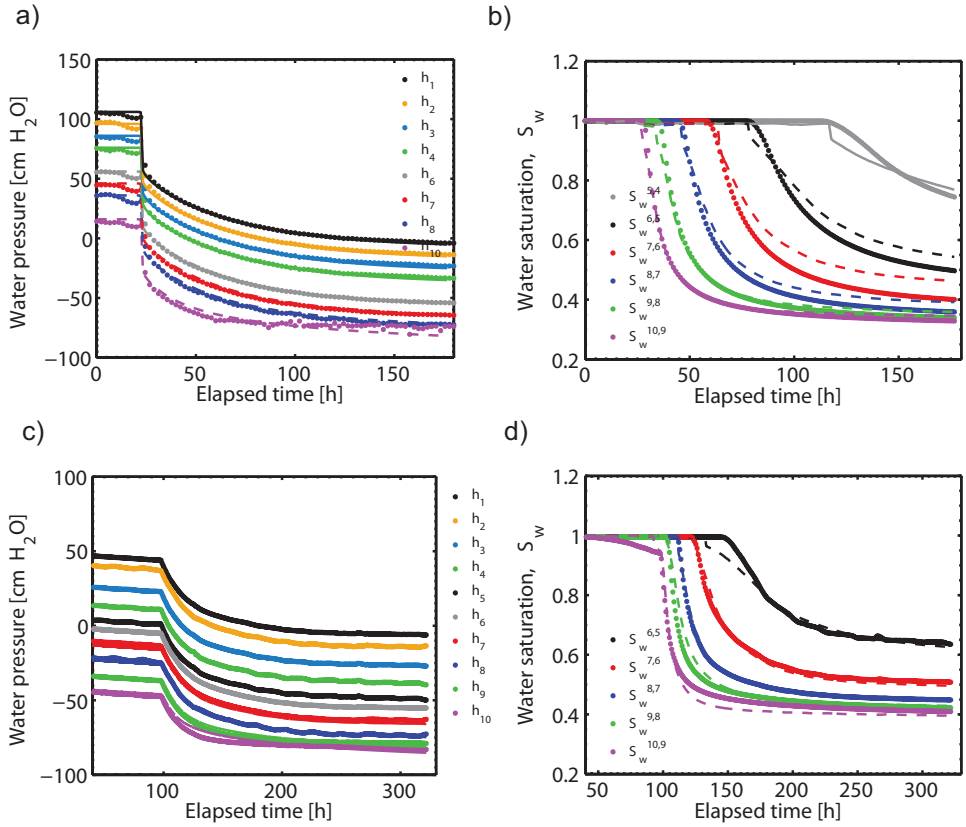

Figure 2. Measured (dots) and computed (lines) water pressure head (expressed in water height) plotted as a function of time, for a) experiment #1 and c) experiment #2. Indice #1 of h_1 indicates the measurement at the bottom, and indice #10 the one at the top of the column. Measured (dots) and computed (lines) water saturation represented as a function of time for b) experiment #1 and d) experiment #2. Exponent i of each ${S_w}^i$ indicates the location of the θ probe inside the column. b) for exp. #1; d) for exp. #2. Drainage started at time 22 hours for experiment #1 and 95 hours for experiment #2.

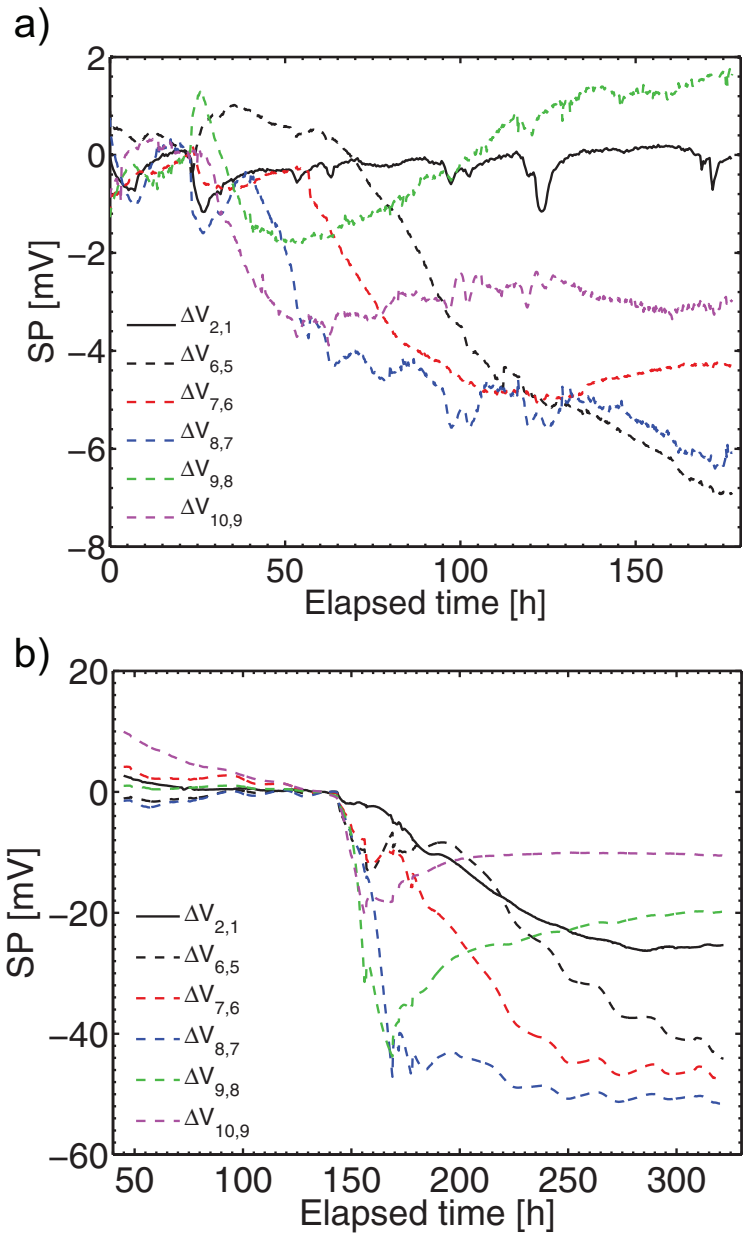

Figure 3. The streaming potentials signals measured with several dipoles along the column during the drainage, plotted as a function of time for a) experiment #1 and b) experiment #2. SP differences at the beginning is zero, because the voltage shift before the experiment was cancelled. Indices indicate the location of dipoles, as $\Delta V_{10,9}$ curve corresponds to SP between electrodes #10 and #9 (see figure 1). Dashed lines correspond to dipoles located in the unsaturated part of the sand at the end of the drainage. The solid black line corresponds to the dipole $\Delta V_{2,1}$ which is always located in the saturated part. Drainage startad at 22 hours and 95 hourrs for exeriments #1 and #2 respectively.

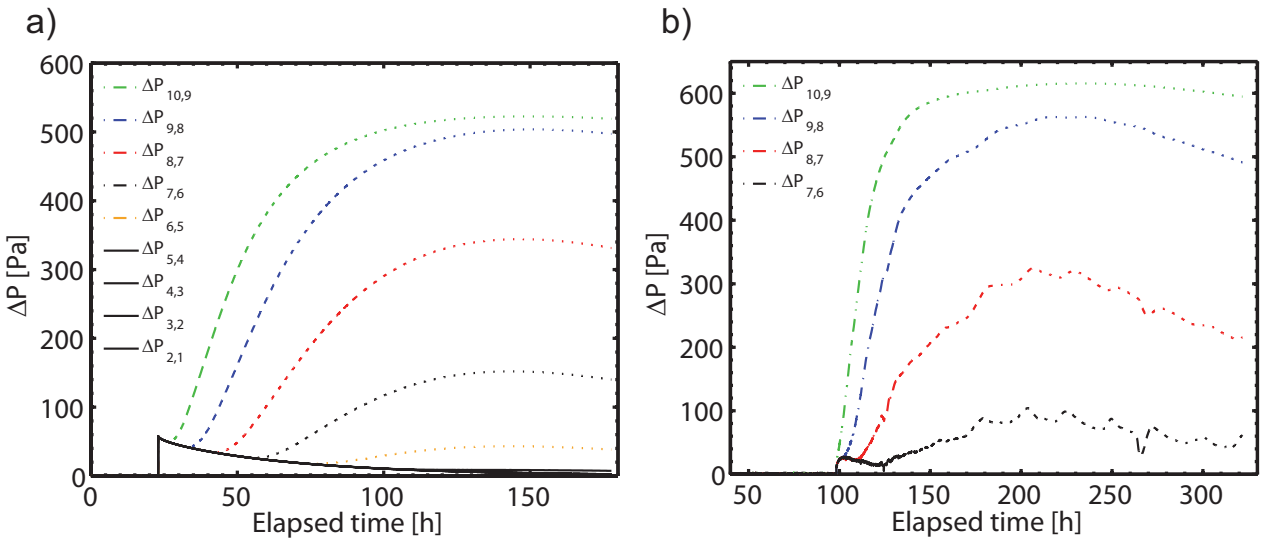

Figure 4. The computed total water pressure in [Pa], deduced from computed water pressures using $\Delta P = \rho_w g(h - z)$ and plotted as a function of time for a) experiment #1 and b) experiment #2. The dashed lines indentify the layers located in the unsaturated sand at the end of the drainage. The black lines identify the layers always located in the saturated part (these lines are mixed up).

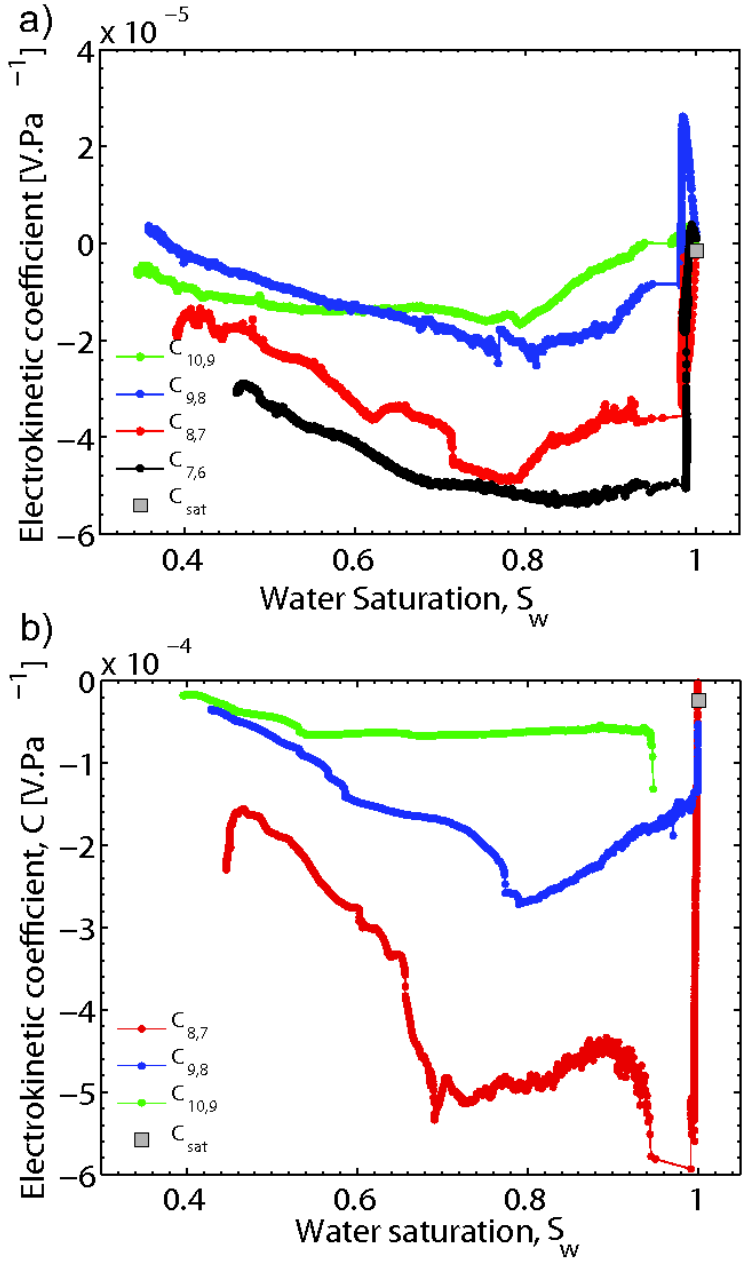

Figure 5. Raw (i.e non normalized) electrokinetic coefficient measurements as a function of measured water saturation for a) experiment #1, with four dipoles presented ($C_{10,9}$, $C_{9,8}$, $C_{8,7}$ and $C_{7,6}$), and for b) experiment #2, with three dipoles shown ($C_{10,9}$, $C_{9,8}$ and $C_{8,7}$). The gray square represent the measured C_{sat} (see Appendix B for details). It is equal to -1.6x10^{-6} V.Pa^{-1} for experiment #1 and to -2.5x10^{-6} V.Pa^{-1} for experiment #2.

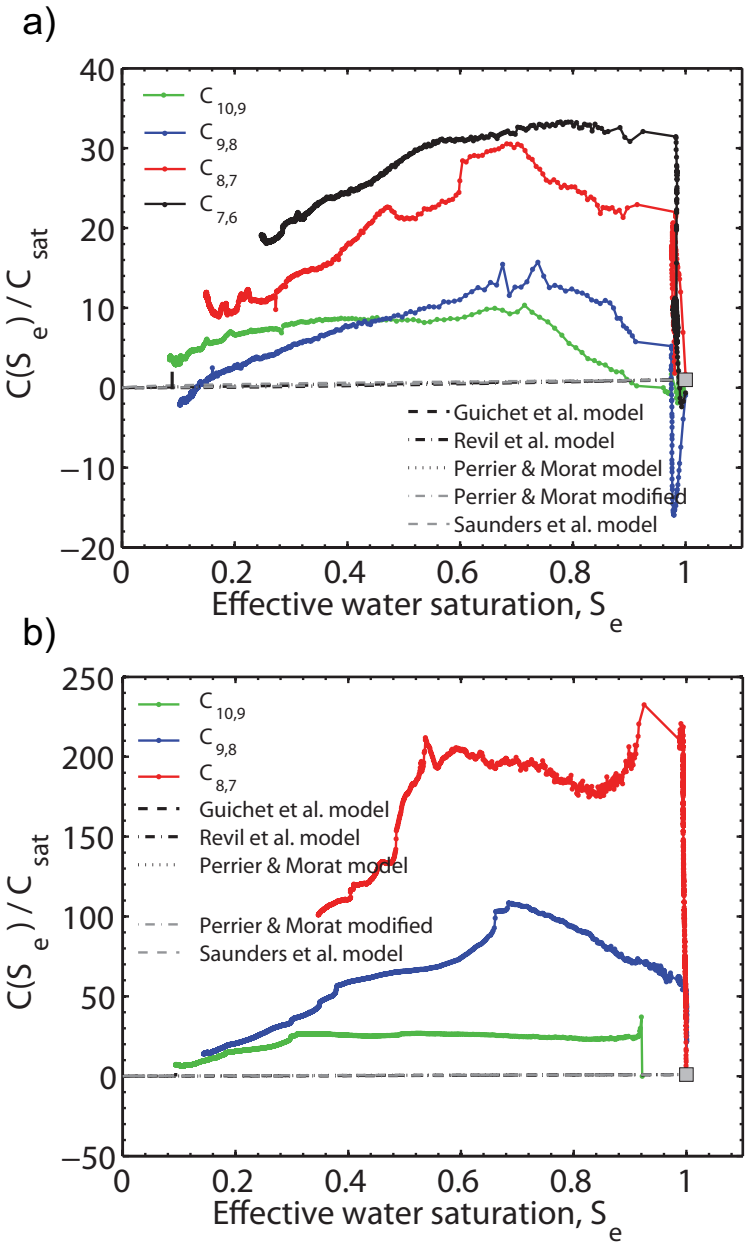

Figure 6. The relative electrokinetic coefficient computed with C_{sat} reported in Table 3, for a) experiment #1 and b) experiment #2. The absolute value of C_{min} is one to two orders of magnitude greater than C_{sat} and implies large maximum values of C_r. The Guichet et al. (2006), Perrier & Morat (2000) and Revil et al. (2007) models are also reported using parameters of the Table 2 ($n = 1.45$ was measured, see B), and Saunders et al. (2008) model is computed for $n_s = 0.5$.

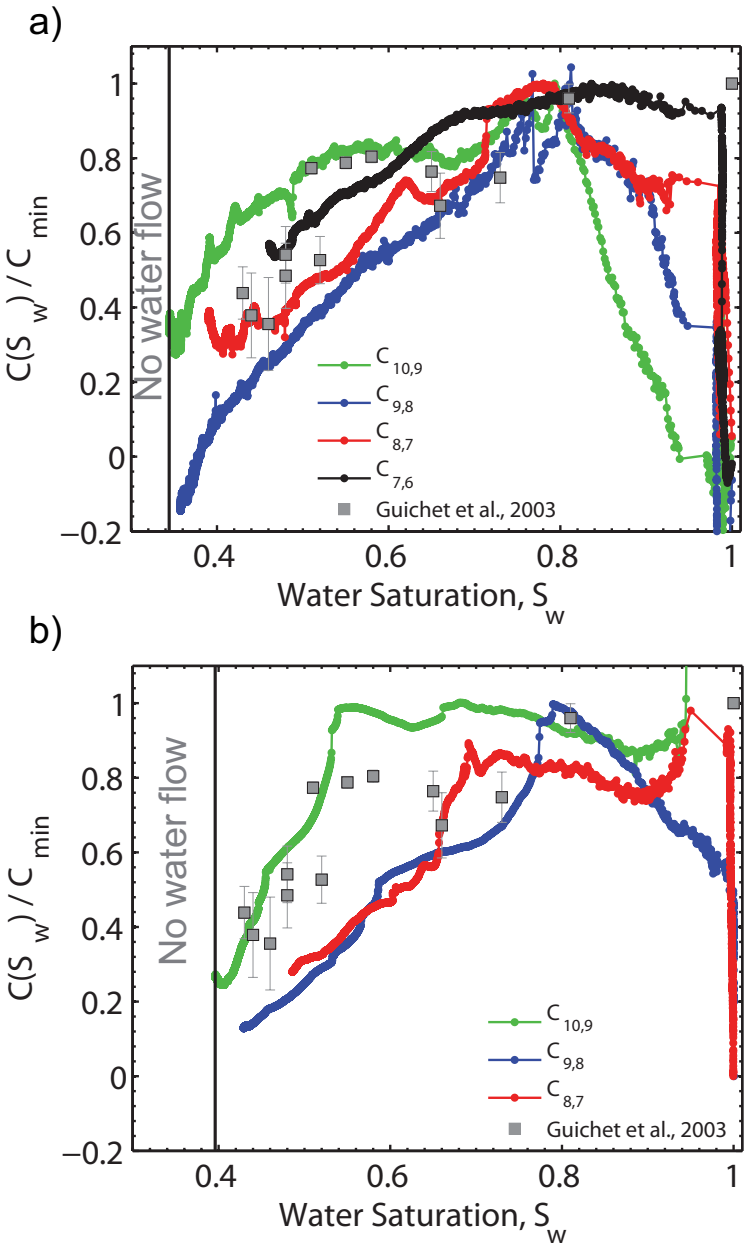

Figure 7. The electrokinetic coefficient computed with equation 17, using measured SP data and computed total water pressure, represented as a function of measured water saturation for a) experiment #1 and b) experiment #2. These values are normalized by the minimum value (equation 18). Only the four dipoles located in the unsaturated sand are plotted for experiment #1 ($C_{10,9}$, $C_{9,8}$, $C_{8,7}$, $C_{7,6}$) and three for experiment #2 ($C_{10,9}$, $C_{9,8}$, $C_{8,7}$). The gray squares represent Guichet et al. (2003) experimental data on sand.

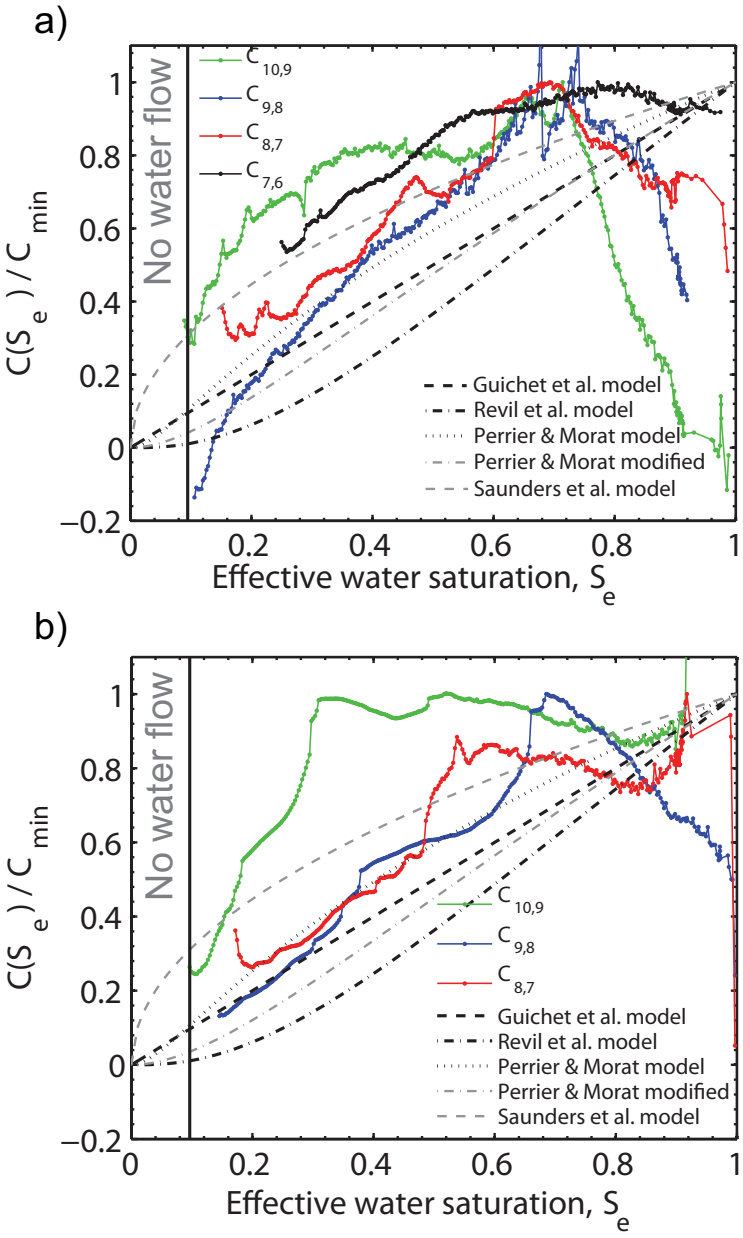

Figure 8. The electrokinetic coefficient deduced from our measurements as a function of the effective water saturation, normalized to the minimum value, for a) experiment #1 and b) experiment #2. The Guichet et al. (2006), Perrier & Morat (2000) and Revil et al. (2007) models of $C_r(S_e)$ are computed using parameters of the Table 2, and Saunders et al. (2008) model is computed with $n_s = 0.5$.

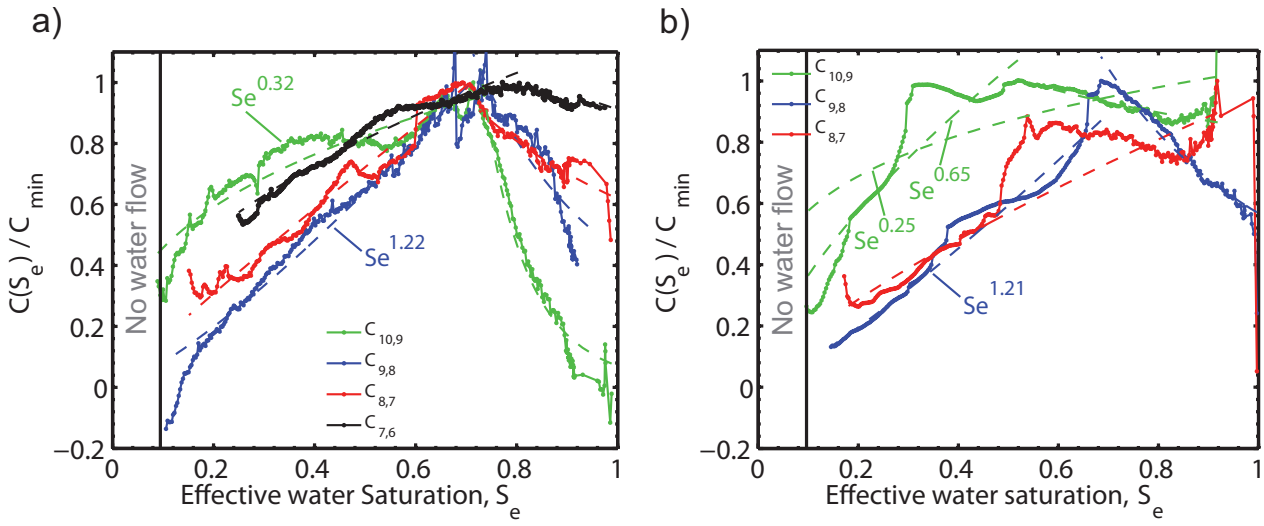

Figure 9. The electrokinetic coefficient deduced from our measurements as a function of the effective water saturation, normalized to the minimum value, for a) experiment #1 and b) experiment #2. The results of least-square adjustments using equation 19 are represented with dashed lines.

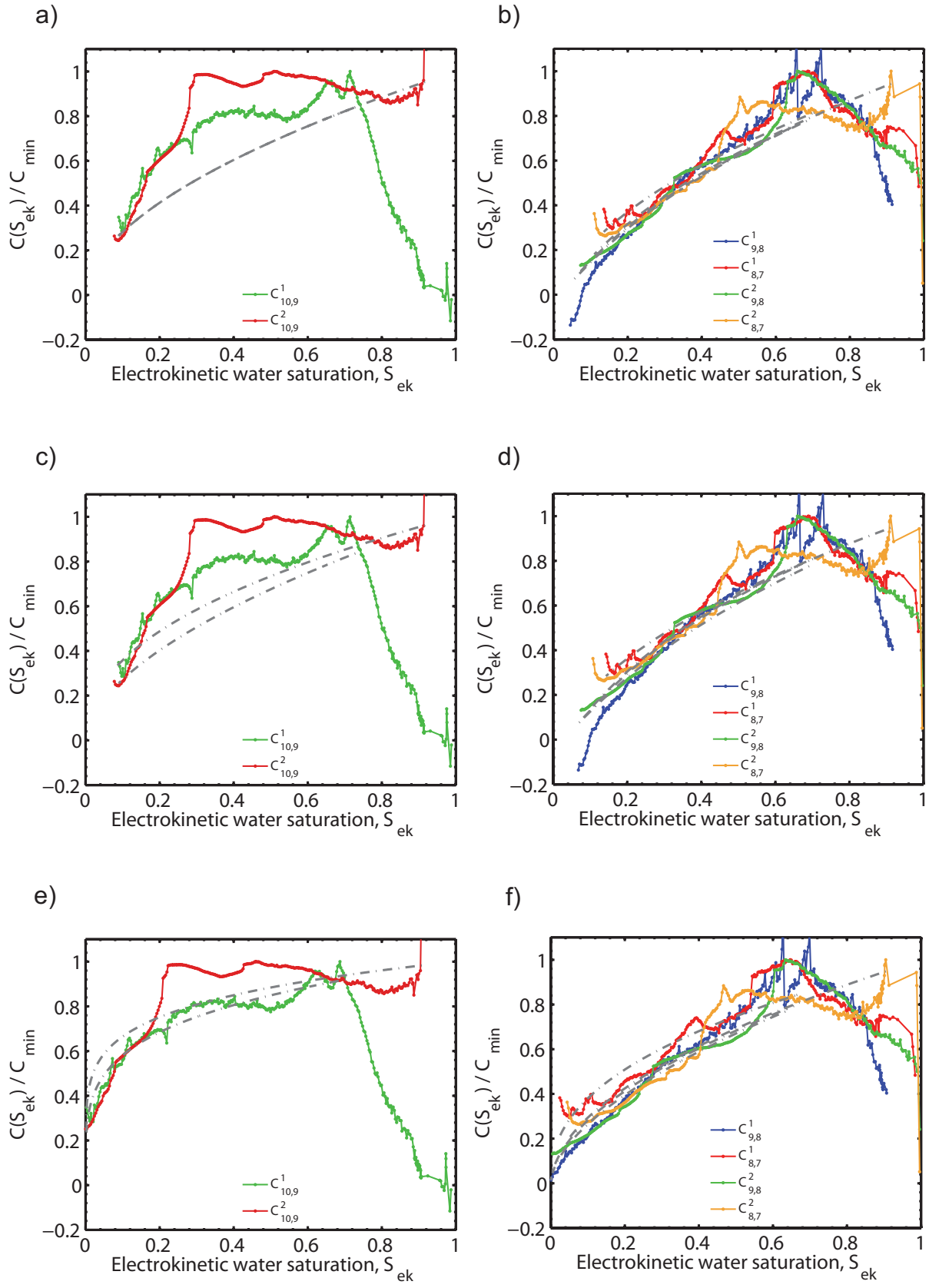

Figure 10. Fit of equations 21, 22 and 25 for dipoles $C^1_{9,8}$, $C^1_{8,7}$, $C^2_{9,8}$ and $C^2_{8,7}$ (b, d, f), and for dipoles $C^1_{10,9}$, $C^2_{10,9}$ (a, c, e). Electrokinetic coefficient data are plotted as a function of the electrokinetic water saturation S_{ek} and normalized to the minimum value. See Table 5 for the values of β and $S_w^{r,ek}$.

APPENDIX A: INSTRUMENTAL AND EXTERNAL FACTORS INFLUENCING SP MEASUREMENTS

We present in this section some test experiments carried out to investigate the different sources of electrical noise on SP measurements. This noise could be induced by acquisition process or by experimental setup.

The first experiments were performed in water to study the influence of water content probes on SP measurements. Actually these probes apply an electrical field to perform the measurements and it could perturb the streaming potential measurements. Some SP measurements were combined to water content measurements (black and red curve) and compared to SP alone (green curve) (A1). The shielded part of SP electrode's cables is connected to a secure ground point on the acquisition unit. We observe that the high frequency noise increases when water content is measured. The amplitude of this noise is around 0.2 mV, which is negligible in regards to the typical SP values presented in this paper. In order to reject anthropogenic noise, the signals are integrated on several periods of the 50 Hz signal. The black signal on the figure is integrated on 100 periods of the 50 Hz, corresponding to 2 s of measurement, and the red one is integrated on 10 periods only. The impact of this integration is important, so that we chose to integrate all SP measurements on 100 periods of the 50 Hz for each experiment. Finally, some more larger fluctuations (around 1 mV) are identified on the red curve, with a 12 hours delay. These variations are linked to temperature fluctuations which are detailed below.

Finally, water content probes have been placed into the column 5 centimeters (see Figure 1) from SP electrodes to minimize their effects.

The same experimental protocol was used to fill the column to ensure the repeatability of all experiments. The column has been filled by imbibition in order to limit the formation

of air bubbles and to ensure a uniform paking. When the sand is dropped into the column, the water volume is maintained larger than the sand volume. Thus, the medium remains saturated and the water content is uniform in the whole column. Finally, a first test drainage is carried out to ensure the sand packing.

The chemical equilibrium stability of the mixture (sand with water) and temperature fluctuations have been monitored during the equilibrium phase, before the drainage experiment. The water electrical conductivity, σ_w, and pH during the chemical equilibrium phase (described in the section 3) are measured in the stocked water and in the outflow water, which is the water sampled at the column exit after flow (Figure A2). We observe the stabilization of both σ_w and pH values after recycling the pore volume four times. This stabilization, considering the measurement accuracy, is obtained after almost 7 days, in the same flow conditions than for the drainage experiment.

Temperature fluctuations have also been monitored, using two thermocouples, inside and outside the column during the first experiment (Figure A3b), and are compared to raw SP measurements (Figure A3a). Some periodical variations linked to day/night cycles are clearly identified on the temperature measurements. The maximum value of temperature fluctuations inside the column is about 2 °C.

Corresponding peaks in the raw SP signals are identified by dashed lines (Figure A3) and clearly correlated to temperature. However, the noise amplitude involved in SP data by temperature fluctuations is negligible, in regards to characteristic SP signals measured during a drainage experiment.

The two experiments presented in this paper are very long (around 3-4 hundred hours), so that it is important not to have a drift in the SP signals.

Raw SP recordings of the first experiment are reported (Figure A4). The first frame represents almost 24 hours of measurements before the drainage start. The second frame repre-

sents more than 40 hours of measurements after the drainage stopped. These two examples show a very stable SP signals for all dipoles when there is no water flow. Moreover, the SP measured with the dipole (2,1) is stable around 1 mV for 400 hours of recording, as we could expect in the part of the column which remains saturated. These examples reject the possibility of electrodes drifting during the experiment and attest their accuracy.

Another example of a long raw SP recording before a drainage experiment not presented in this paper shows a quite stable electrical potential values during 50 hours after a long equilibrium phase (Figure A5). This example is representative of recorded signals of different phases during an experiment.

We concluded from all these test experiments that the instrumental and external sources of electrical noise are small enough to allow us to detect a streaming potential induced by a drainage experiment.

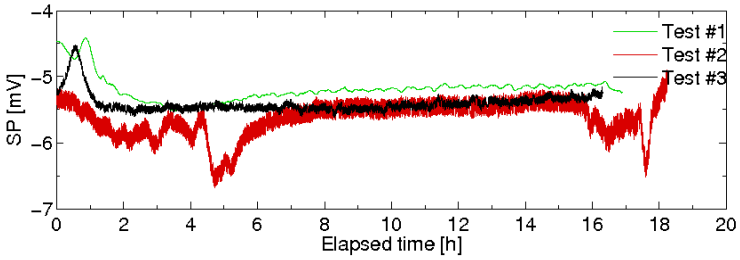

Figure A1. Test SP signals measured in water. The green curve represents SP without any other measurements, the red curve represents SP measured without the ground connection, and the black and red curve represent SP measurements combined to water content measurements. All these signals are integrated on 100 periods of 50 Hz.

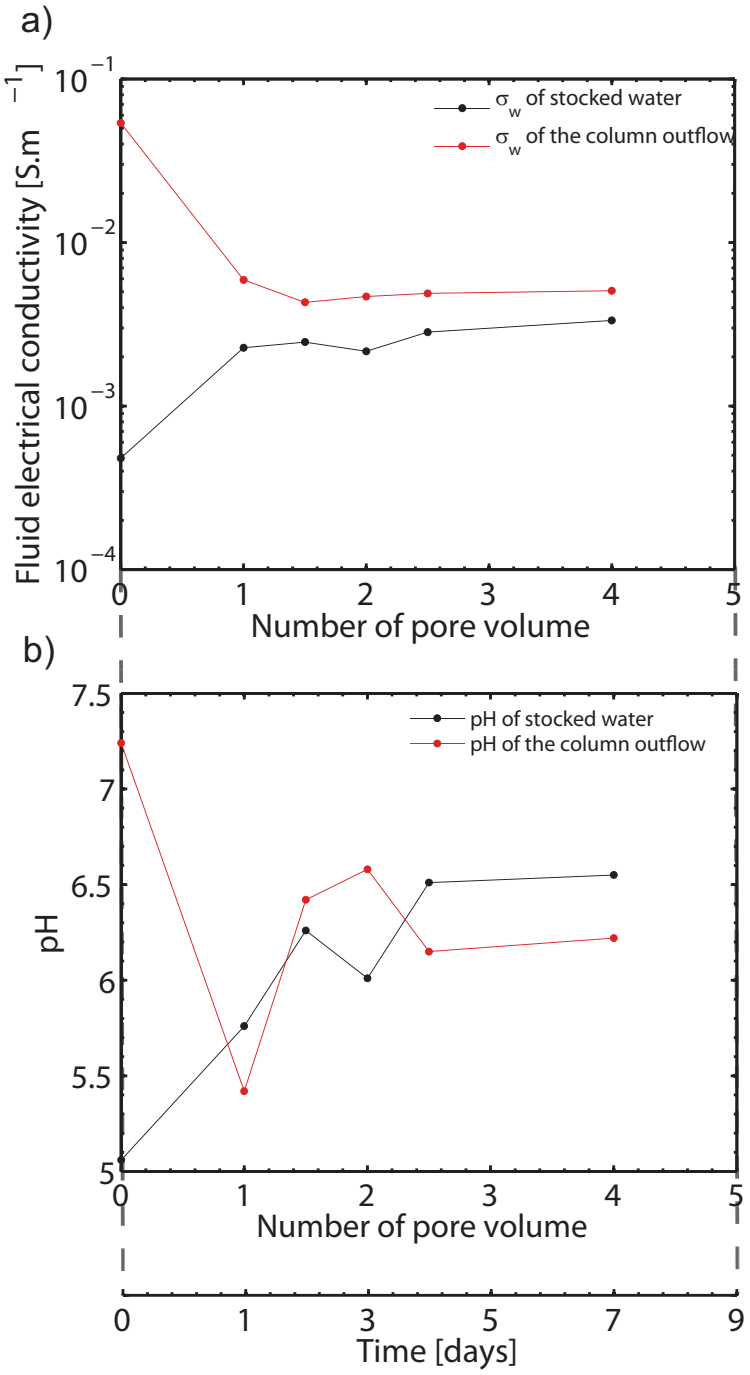

Figure A2. Water electrical conductivity and pH measured during the equilibrium phase of the first experiment, in the stocked water and in the outflow water. The flow conditions are the same than those during a drainage experiment.

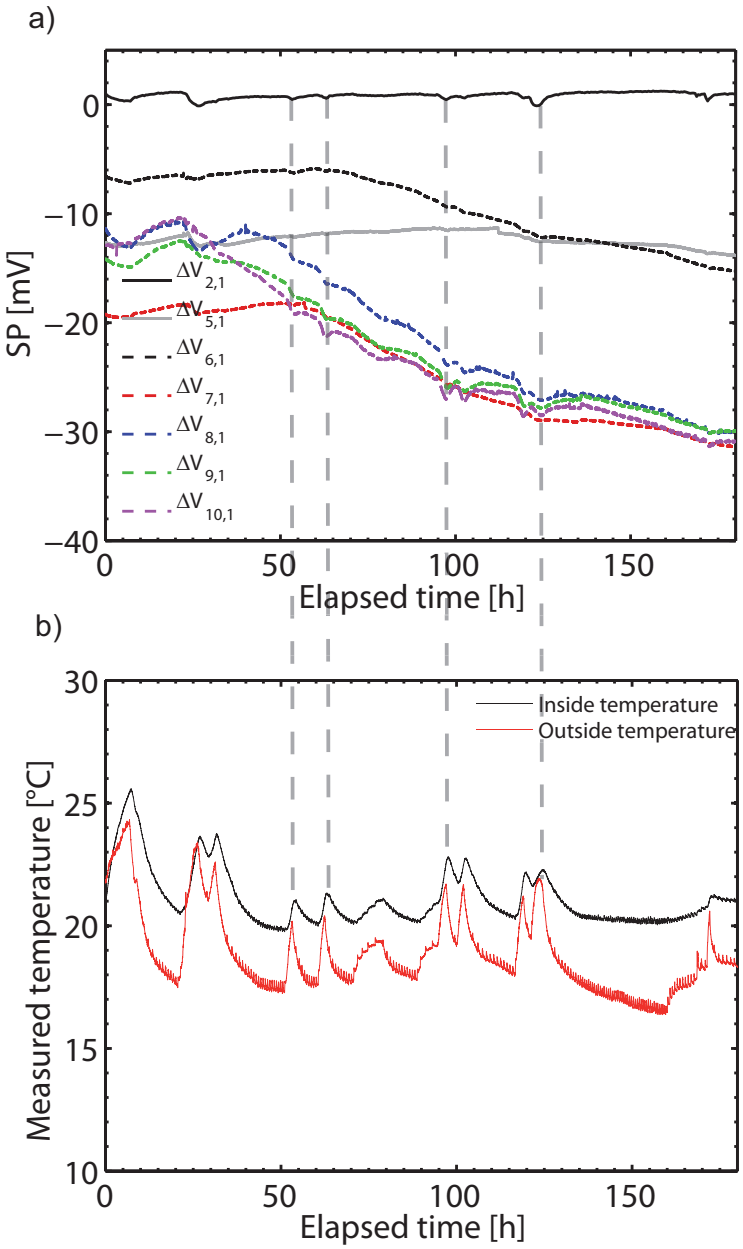

Figure A3. Raw SP measurements of the first experiment (a) and temperature monitored inside and outside the column at the same time (b).

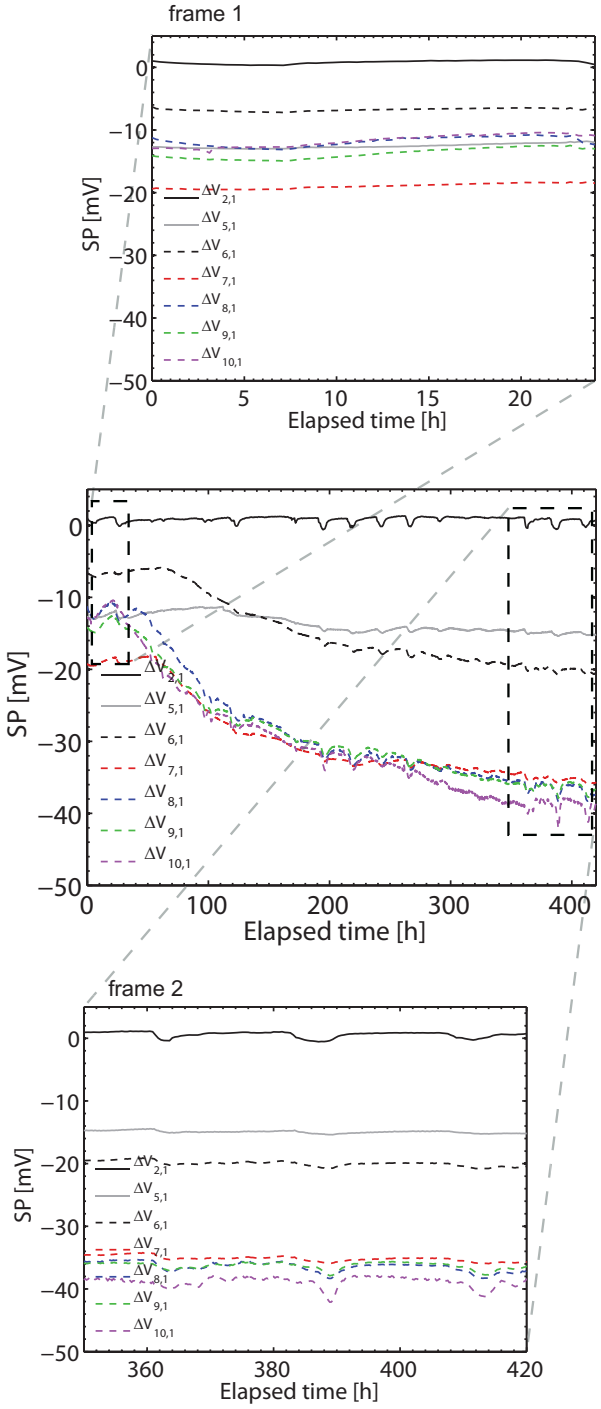

Figure A4. Raw SP measurements for the first experiment. The frame #1 is a zoom on the first 24 hours of the recording (before the drainage start), and the second frame is a zoom on the last 40 hours of the recording (after the flow stop).

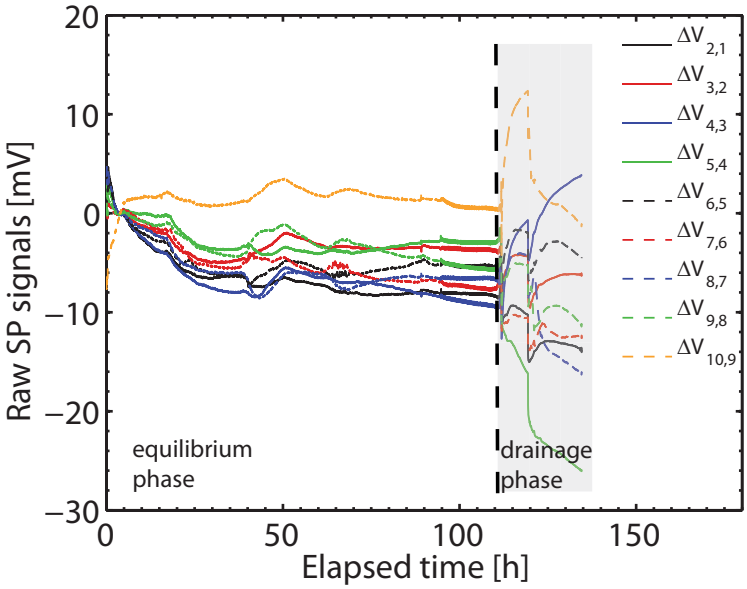

Figure A5. An example of experimental recording during the equilibrium phase. A 30 hours stable phase is identified just before the drainage start.

APPENDIX B: ELECTRICAL AND ELECTROKINETIC CARACTERIZATION OF THE SAND

The C_{sat} value can be measured in steady-state saturated flow. Streaming Potential (SP) is measured for several applied pore pressures within a sample of sand (Figure A6a). These measurements were performed using another experimental setup (Jouniaux et al. 2000), to be able to apply large enough pressure differences (up to 30000 Pa) to induce a measurable electrokinetic coefficient, which was $-3\text{x}10^{-7}$ V.Pa^{-1} (with $\sigma_w = 0.055$ S.m^{-1}). The slope of the regression leads to the value of C_{sat}. These measurements have been made at a higher water salinity than the one observed in both experiments presented in this paper. Assuming that the Helmholtz-Smoluchowski equation is valid, we inferred the C_{sat} values corresponding to the conductivities of the two experiments of this paper. This calculation leads to $C_{sat} = -1.6\text{x}10^{-6}$ V.Pa^{-1} (with $\sigma_w = 103.2\text{x}10^{-4}$ S.m^{-1}) for the first one and $C_{sat} = -2.5\text{x}10^{-6}$ V.Pa^{-1} (with $\sigma_w = 66.4\text{x}10^{-4}$ S.m^{-1}) for the second one. Measurements of C_{sat} performed on sand and sandstone samples collected in the literature are shown as a function of the water electrical conductivity, σ_w (Figure A6b). The regression leading to $C_{sat} = 10^{-8}.\sigma_w^{-1}$ shows that our values of C_{sat} are in the general trend deduced from other studies on sand and sandstones.

Raw electrokinetic coefficient computed through equation 2, using measured SP and computed ΔP (Figures 3 and 4 respectively), are reported (Figures A7a and b). No water flow was measurable at $\simeq$ 140 hours and $\simeq$ 190 hours after the drainage start for experiment #1 and #2 respectively. At this step, measured water-content and water pressures stopped to decrease and kept stable (see Figure 2). Then, the minimum of water saturation was reached for all the dipoles. Thus, electrokinetic coefficient data presented as a function of water

saturation in this paper correspond to $\simeq$ 140 hours and $\simeq$ 190 hours of measurements from the drainage start. We can also observe on these Figures the scattering of the measurements at the begining of the experiment #1 which we detail below.

In addition, we propose a statistical study of our dataset to estimate its uncertainty. We applied a sliding window to the $C(S_w)$ dataset. The width of the window is defined in terms of water saturation interval $S_w = 0.05$. This value corresponds to the error on water saturation measurements. In each window we analysed the measurements distribution as an histogram. The obtained distributions were non symmetric (as gaussian distribution for instance), so that we decided to represent the median value of the distribution in each window (colored circles in the Figure A8). We computed the error bars using the minimum and the maximum value of $C(S_w)$ in each window. Thus, error bars include 100% of the uncertainty linked to all the noise sources we can not control during the experiment.

The uncertainty is maximum at the beginning of each experiment (Figure A8). We observe that the inferred C_{sat} is included in error bars. Futhermore, error bars also include the zero when some signals change in sign at very low saturations. This analysis confirms that our measurements are precise and accurate enough to follow the electrokinetic coefficient behaviour as a function of water saturation.

The electrokinetic coefficient models computed in Section 5 need the Archie saturation exponent n to be known. Rather than to choose n from some published values, we decided to measure electrical resistivity of the unsaturated sand in a small-scale column (already used for Theta probe calibrations). Nine sand mixtures were prepared by weight to obtain nine different homogeneous unsaturated media. The values of θ varies from θ_r to θ_s to ensure a good coverage of the whole saturation domain. We also measured the porosity (equivalent to θ_s) which was equal to 0.36. Measurements of electrical resistance were carried out with circular stainless steel (same diameter than the column) placed at each extremity,

and using an impedancemeter (Agilent 4263b) combined with the same acquisition system than for experiments #1 and #2. Thus, the simple and short cylindrical geometry of this experiment allowed us to easily convert raw electrical resistance values in terms of true electrical resistivity ρ_{meas}. The values ρ_{meas} normalized by the measured water electrical resistivity are shown as a function of water saturation (Figure A9). Then, Archie's law was fitted to the data in a least square sense, and results gave $n = 1.45$ for the second Archie exponent.

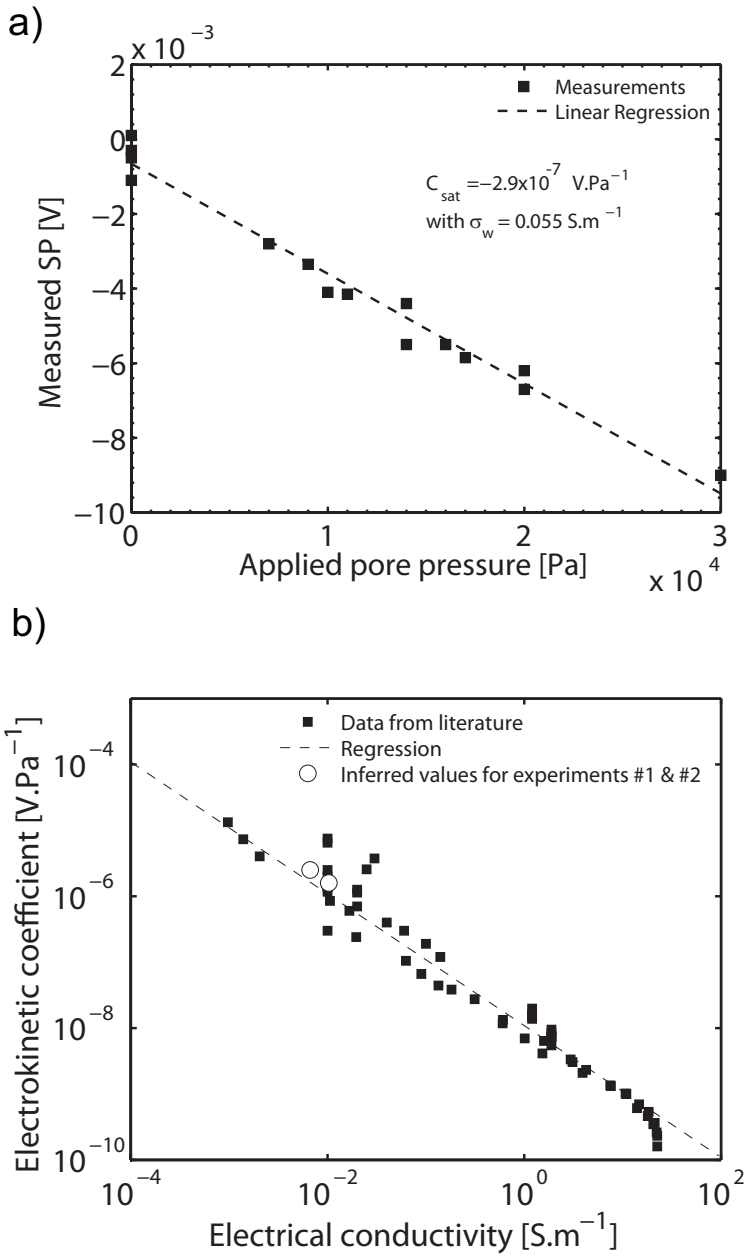

Figure A6. a) SP measured on Sifraco NE34 sand sample as a function of applied pore pressures. The slope of the regression (black dashed line) leads to the value of the electrokinetic coefficient at saturation, $C_{sat} = -2.9\text{x}10^{-7}$ V.Pa^{-1} for water conductivity $\sigma_w = 0.05\text{x}10^{-2}$ S.m^{-1}. b) The inferred values of C_{sat} at conductivities used in exp.#1 and #2 are represented by empty circles. Comparison with data collected (in absolute terms) on sands and sandstones at pH $7-8$ (when available) from Ahmad (1964), Guichet et al. (2003, 2006), Ishido & Mizutani (1981), Jaafar et al. (2009), Jouniaux & Pozzi (1997), Li et al. (1995), Lorne et al. (1999a), Pengra et al. (1999), Perrier & Froidefond (2003). The regression (black dashed line) leads to $C_{sat} = -1,1\text{x}10^{-8}$. σ_w^{-1} V.Pa^{-1}

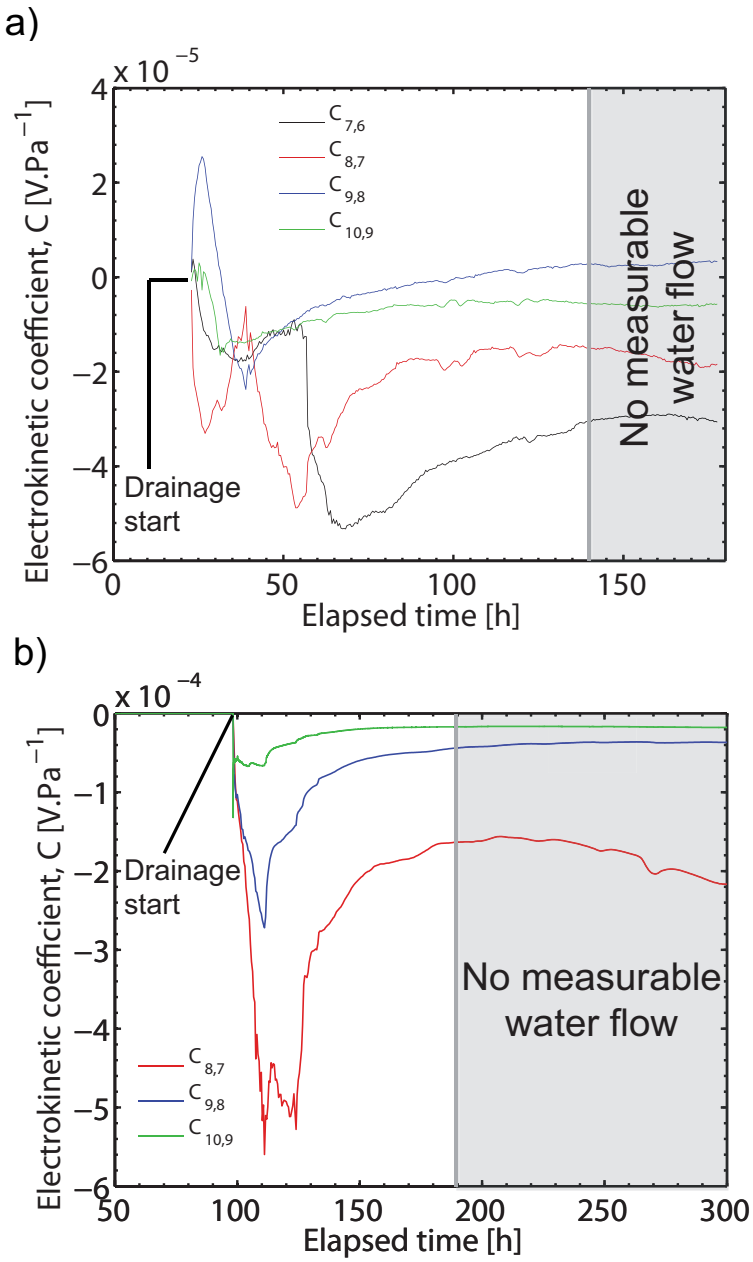

Figure A7. The raw electrokinetic coefficient measurements deduced from measured SP and computed ΔP as a function of time. a) Data from dipoles $C_{10,9}$, $C_{9,8}$, $C_{8,7}$, and $C_{7,6}$ are shown for experiment #1. b) Data from dipoles $C_{10,9}$, $C_{9,8}$, $C_{8,7}$ are shown for experiment #2.

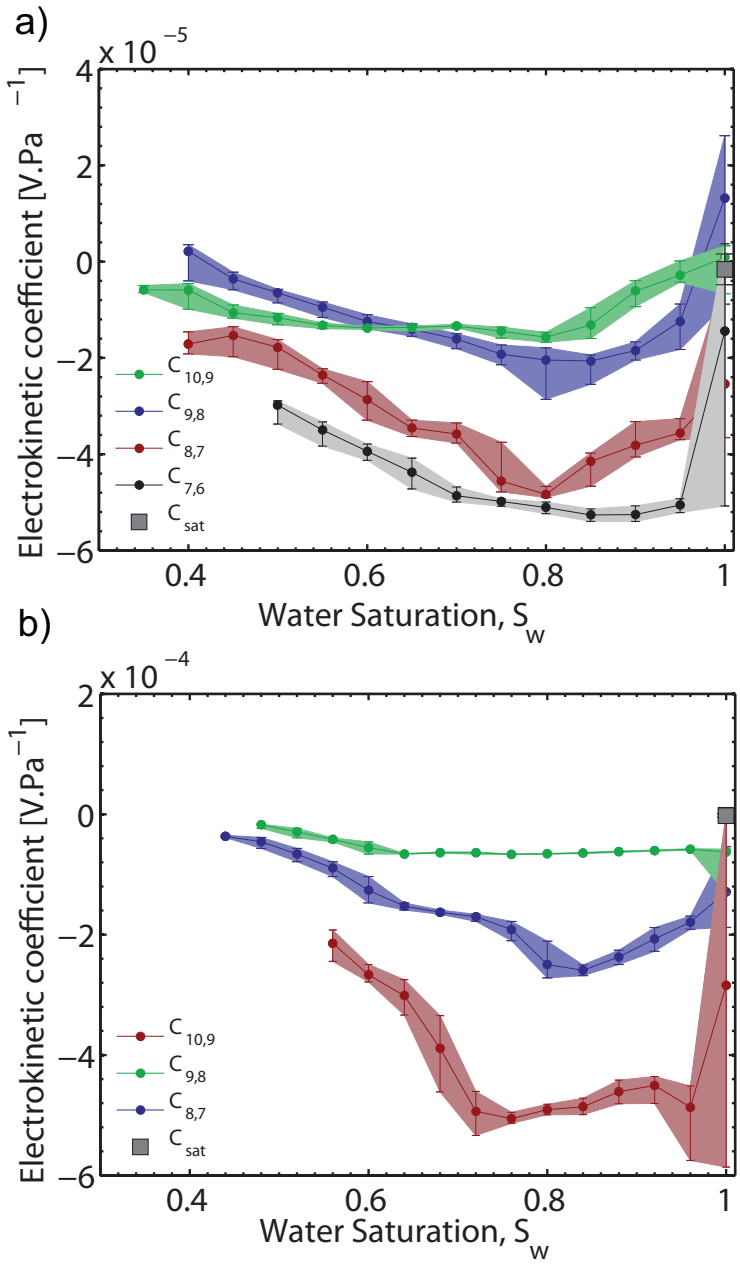

Figure A8. Statistical study of the un-normalized values of the electrokinetic coefficient measurements. A sliding window of 0.05 width is applied to the dataset. The median of the distribution is chosen for each window to represent the data. The error bars correspond to the minimum and maximum values of the distribution in each window. The inferred values of C_{sat} are represented by squares.

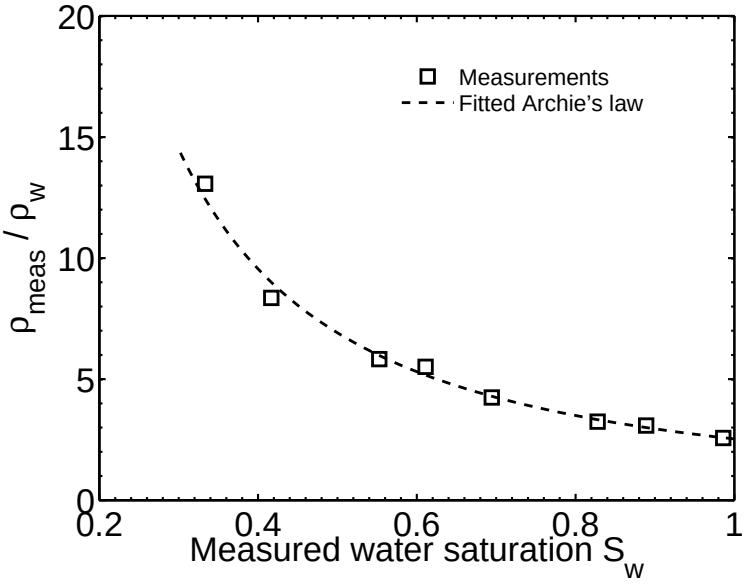

Figure A9. True electrical resistivity of the sand as a function of water saturation. The black squares represent measured ρ_r/ρ_w for nine water/sand mixtures. The water-content was controlled by weight. The black dashed line is the best Archie's law fitting the data. Results lead to $n = 1.45$ for the Archie saturation exponent.